

**Solar wind – Variability, evolution to Earth
and influence
on the terrestrial magnetic field**

Doctoral thesis in physics

Malte S. Venzmer

University of Göttingen

Institute for Astrophysics

January 2012 – Dez? 2017

Supervisor:
Dr. Volker Bothmer

Referees:
Prof. Dr. Ansgar Reiners
Prof. Dr. ??

“Despite the ‘Dr.’ before his name, he had completed no course of study and received no degree. When people tried to pin him down about this, he would say that the letters were merely an abbreviation of his first name - Drummond - which he did not use. But it was as ‘Dr.’ Sam Laserowitz that he appeared in a number of science-fiction magazines; he was also known, in the circles of the fans of that genre, as a lecturer, and spoke on ‘cosmic’ themes at their many conferences and convention. Laserowitz’s speciality was earthshaking discoveries, which he happened upon two or three times a year. [...] We really have no idea what a multitude of con men and crackpots inhabit the domain that lies halfway between contemporary science and the insane asylum.”

Excerpt from Stanisław Lem 1968, *His Master’s Voice* (Lem & Kandel 1984, p. 38).

version log:

- 1 2013-11-06
- 2 2013-11-07 inserted lem excerpt
- 3 2014-09-01 outlined introduction structure and appendix key words
- 4 2014-09-11 bibtex included, lem excerpt citet
- 5 2014-09-12 included italic titles in bibliography
- 6 2015-01-12 worked on introduction structure and included magnetic butterfly diagram
- 7 2015-05-04 first printout, small additions
- 8 2015-07-03 coupling functions, content structure
- 9 2015-09-09 Alfvén wave velocity formula
- 10 2015-09-10 Appendix physics: Alfvén and compressional MHD waves, plasma beta; citation sources Cranmer2005, Kivelson1995
- 11 2015-09-15 CGAUSS work overview; DQCS model figure
- 12 2015-09-16 magnetic energy density is the same as magnetic pressure, abbreviations
- 13 2015-09-30 empirical solar wind model plots in analyses, figure label [Figure 4.2 Text]
- 14 2015-10-02 table column decimal alignment; set caption width
- 15 2015-10-05 table units; radial parameter (N, T) profiles in literature
- 16 2015-10-06 literature radial electron density models; log-normal distribution
- 17 2015-10-07 log-normal formulae
- 18 2015-10-08 log-normal fit
- 19 2015-10-09 shape fit parameter table; radial variance fitting
- 20 2015-10-14 variance fit values; log-normal citation Bronstein
- 21 2015-10-19 radial distribution width fitting; clarifying of solar wind model formulae structure and naming variables
- 22 2015-10-20 log-normal distribution width factor changes the shape!
- 23 2015-10-23 log-normal distributions mu and sigma plot
- 24 2015-10-30 new sigmafit2 figures implemented; formulae adaption
- 25 2015-11-02 reason for use of log-normal function
- 26 2015-11-20 single log-normal shape fit; not chisquare - SSR; R^2 in appendix
- 27 2015-11-26 reduced SSR into tables; table column aligning
- 28 2015-12-02 smoothing SSR integration
- 29 2015-12-07 integrating structure remarks from printout
- 30 2015-12-09 splitting analyses chapter into two; browsing folders for usable things for thesis
- 31 2015-12-10 integrating citations and references

-
- 32 2015-12-16 integrating citations and references
 - 33 2015-12-18 solar wind structures list of Richardson
 - 34 2016-02-02 sws distributions
 - 35 2016-02-11 basics structure
 - 36 2016-02-12 analyses questions
 - 37 2016-02-15 analyses structure; in situ, near-Sun
 - 38 2016-02-16 Kp index internal resolution
 - 39 2016-02-17 Bartels1962; non-breaking hyphen shorthand implemented
 - 40 2016-02-18 analysesI structure
 - 41 2016-02-25 abstract
 - 42 2016-02-26 english comma
 - 43 2016-03-01 Bartels Kp origin paper, bibtex reference
 - 44 2016-03-02 abstract
 - 45 2016-03-03 Planck paper
 - 46 2016-03-07 formation of stars
 - 47 2016-03-08 formation of stars
 - 48 2016-03-16 solar interior structure
 - 49 2016-03-17 solar interior structure
 - 50 2016-03-18 solar surface
 - 51 2016-03-22 Astronomical Almanac citation
 - 52 2016-03-23 solar core definition
 - 53 2016-03-26 sunspots
 - 54 2016-03-29 Sun interior figure
 - 55 2016-03-30 solar composition
 - 56 2016-03-31 Sun interior figure finished; chromosphere
 - 57 2016-04-01 Sun atmosphere figure finished
 - 58 2016-04-03 chromosphere, corona, CV
 - 59 2016-04-07 CV
 - 60 2016-04-08 CV; heliosphere
 - 61 2016-04-09 corona; heliosphere
 - 62 2016-04-11 heliosheath magnetic bubbles; Opher2011
 - 63 2016-04-12 heliosphere; voyagers; Gurnett2013
 - 64 2016-04-13 solar wind effects, solar rotation
 - 65 2016-04-14 analysesI sws structure draft plots
 - 66 2016-04-15 analysesI concept work
 - 67 2016-04-19 incorporate annotations from processed printout
 - 68 2016-04-21 incorporate annotations from processed printout II
 - 69 2016-04-22 incorporate annotations from processed printout III
 - 69 2016-04-23 updated .bst file (for displaying arXiv id); implemented optional url displaying for electronic version; Kp year variations
 - 70 2016-04-24 Kp frequency by month statistics and plot; Sun and Earth tilt plot
 - 71 2016-04-25 solar cycle extrema dates literature
 - 72 2016-04-27 Kp semi annual variation, Rangarajan1997
 - 73 2016-05-01 Kp frequency by year
 - 74 2016-05-04 Kp + SSN plot; ACE data errors/gaps; log-normal plot; differential rotation plot
 - 75 2016-05-05 aggregate correlation coefficient tables, CME fraction plot
 - 76 2016-05-06 overall sws fractions
 - 77 2016-05-17 figure sw frequencies by year; restructured solar wind distributions section; formal cover page
 - 78 2016-05-20 Earth-Sun distance; JPL web interface
 - 79 2016-05-31 GSM system
 - 80 2016-06-10 Offline Anmerkungen einarbeiten
 - 81 2016-06-12 LaTeX Earth symbol package
 - 82 2016-06-13 numbers=noenddot
 - 83 2016-06-14 references removed comma before ampersand; offline Anmerkungen einarbeiten; thesis_raw version
 - 84 2016-06-17 gnuplot figures and latex; latex document style options
 - 85 2016-06-19 header implemented
 - 86 2016-06-20 minor things; introduction
 - 87 2016-06-23 solar tilt axis

88 2016-06-24 solar rotation
89 2016-07-12 magnetosphere temp figure; analyses: solar wind model
90 2016-07-13 lognormal spelling
91 2016-07-14 constant mass flow rate
92 2016-07-18 line-up periods
93 2016-07-19 line-up periods table
94 2016-07-20 redone line-up analysis
95 2016-07-21 line-up tables
96 2016-07-22 line-up fit function plots; coefficient table
97 2016-07-22 line-up sw types and period plots; overview plot
98 2016-07-24 line-up averaging and justification
99 2016-07-29 line-up rework
100 2016-07-30 line-up structure
101 2016-07-31 line-up table
102 2016-08-02 line-up structure
103 2016-08-03 line-up fits and table
104 2016-08-04 insert offline comments
105 2016-08-15 literature radial sw functions
106 2016-08-18 work offline comments in
107 2016-08-19 work offline comments in
108 2016-08-28 analyses II rework structure
109 2016-08-31 analyses II rework structure
110 2016-09-01 analyses II rework figures
111 2016-09-02 analyses II rework structure
112 2016-09-03 Helios latitude dependency
113 2016-09-04 extrapolation model fit parameter table; Helios latitude dependence
114 2016-09-06 work in offline comments
115 2016-09-14 implement median and mean in composite fit table; create kile project for thesis; url and raw fork
116 2016-09-17 Ulysses polar plot; solar distance plots
117 2016-09-18 for solar distance and latitude -> 4-panel figures created and implemented; appendix figures
118 2016-09-20 latitude plots updated
119 2016-09-26 single lognormal fit figure
120 2016-09-27 minor tweaks in analyses II
121 2016-09-29 simple fit table errors; table style
122 2016-10-05 lognormal fit errors for tables
123 2016-10-10 line-up passing remarks from AP
124 2016-10-12 siunitx package incorporated
125 2017-01-04 package fancyhdr replaced with scrlayer-scrpage; offline comments for Basics + Data incorporated
126 2017-01-06 package floatrow included for figure side captions; some cites; magnetometer
127 2017-01-08 sun figure updates and new ion energy spectrum figure incorporated
128 2017-01-13 offline comments, new chapter order
129 2017-01-18 activated hyperref package; included autoref and eqref; adjusted link colors; header links
130 2017-02-02 offline comments
131 2017-02-03 offline commtents II, eclipse image
132 2017-02-06 basics figures with floatrow; flow structure
133 2017-02-07 ion energy spectrum figure
134 2017-02-09 Helios mission ssn plot
135 2017-02-12 offline comments
136 2017-02-13 section number link to toc; offline comments
137 2017-02-14 eclipse and magbfly figure captions
138 2017-02-16 offline comments
139 2017-02-19 coronal heating and sw acceleration
140 2017-04-22 set up git repository
141 2017-04-23 incorporate offline comments
142 2017-04-26 bipolar region draft
143 2017-04-27 magnetic layer Ossendrijver2003
144 2017-06-29 magnetosphere figure drafts implemented
145 2017-07-16 streamlined content - including paper and chapter2

146 2017-07-22 streamlined duplicate content
147 2017-10-05 Kp index data
148 2017-10-28 geomagnetic indices; Kp index; Kp to ap table
149 2017-10-29 Kp index
150 2017-10-30 OMNI s/c coverage figure
151 2017-10-31 OMNI s/c coverage figure upgrade; data set timeline figure

2017-10-31 15:40 – last save

Abstract

This thesis analyzes the solar wind variability, its properties, how they evolve on their way from the Sun and how strong the solar wind's internal structures impact the terrestrial magnetosphere. In situ data from the near-Earth OMNI data set and sunspot number data is used for deriving a functional dependence of the solar wind parameters with the state of the solar cycle. Data from the Helios missions is analyzed and empirical solar wind distance dependencies for 0.3–1.0 au are derived. In view of the planned near-Sun spacecraft mission Solar Probe Plus, additionally the solar wind environment is estimated down to < 10 solar radii. In situ solar wind measurements from the near-Earth OMNI data set are analyzed together with time series of the planetary geomagnetic disturbance indicator K_p . Correlation functions are compiled with regard to forecast the magnitude of the geomagnetic disturbances from solar wind measurements.

Contents

1	Introduction	1
2	Basics	3
2.1	Solar composition	3
2.2	Solar dynamics	6
2.3	Solar wind	10
2.4	Heliospheric magnetic field	10
2.5	Solar wind properties and structures	11
2.5.1	Solar wind plasma	11
2.5.2	Slow solar wind	11
2.5.3	High speed streams	11
2.5.4	Stream interaction regions	12
2.5.5	HCS / HPS	12
2.5.6	Coronal mass ejections	12
2.6	Space weather	12
2.6.1	Solar influence on Earth	13
2.6.2	Magnetosphere	13
2.6.3	Geomagnetic indices	15
2.6.4	Solar wind–magnetosphere coupling	15
3	Data	17
3.1	Instruments	17
3.1.1	Magnetometer	17
3.1.2	Plasma detector	17
3.2	Data sources	18
3.2.1	Sunspot number	18
3.2.2	K_p index	18
3.2.3	OMNI data set	20
3.2.4	Helios probes	21
3.2.5	Parker Solar Probe	23
3.2.6	Real-time solar wind data	23
4	PaperMVVB	25
4.1	Literature	25
4.2	Seasonal solar wind variations	25
4.3	Latitude dependency	26
4.4	Radial evolution of solar wind structures	27
4.5	Solar distance dependency—theory	27
4.6	flux conservation	28
4.7	sw parameters and precision	29
4.8	other	29
5	Helios radial line-up passings	31
6	chapter2	37
6.1	Solar wind interaction processes with the magnetosphere	37
6.2	Solar wind–magnetosphere coupling functions	37
6.3	Parameter selection	37
6.4	Data selection	38
6.5	Solar cycle influence	38
6.6	CME correlations	38
6.7	Solar wind structure analyses	38
6.8	Forecast	39

7 Discussion and results	41
8 Summary and outlook	43
A Physics	45
A.1 Electromagnetism	45
A.2 Solar wind pressures	45
A.3 Plasma beta	45
A.4 Alfvén waves	46
A.5 Solar surface differential rotation	46
A.6 Earth orbit geometry	47
A.6.1 Solar distance	48
A.6.2 Solar rotation axis tilt	48
A.6.3 Earth tilt	48
A.7 Coordinate systems	48
A.7.1 Geocentric Solar Ecliptic	49
A.7.2 Geocentric Solar Magnetospheric	49
A.7.3 Heliographic Inertial	49
B Math	51
B.1 Correlations	51
B.2 Lognormal distribution	51
B.3 Goodness of fit	52
B.4 other	53
C Glossary	55
C.1 Astronomical constants	55
C.2 Symbols	55
C.3 Abbreviations	55
References	57
Acknowledgments	61
Curriculum vitae	63

1 Introduction

Introductory text -> Motivation for

- time variation analysis
- distance analysis
- K_p impact analysis

Synopsis (chapters, content)

This thesis merges the solar wind analyses of its variation in time (autorefch:), its evolution to Earth (chapter XX) and its impact on the magnetosphere (chapter XX). The solar wind model derived in the first two chapters is used together with SSN predictions to estimate the near-Sun solar wind environment the planned SPP spacecraft will encounter during its mission, beginning in 2018. Lists of constants, symbols and abbreviations used in this thesis are located in the appendix.

2 Basics

First this chapter sketches the Sun's origin, inner structure, atmosphere and heliosphere. Then the Sun's dynamics with its magnetic field variations and solar cycle are outlined (including differential rotation, magnetic field generation, solar cycle, quiet/active Sun characteristics on surface and solar wind with HMF consequences). The solar wind and its characteristic structures are described. Further, the solar influence on Earth, on its magnetosphere and other space weather effects are portrayed.

2.1 Solar composition

13.8 billion years ago the Big Bang formed our universe. The energy density of our universe consists of 69.1% dark energy, 25.9% dark matter and 4.9% baryonic matter according to calculations using the inflationary Λ CDM cosmology together with the latest CMB temperature measurements ([Planck Collaboration et al. 2016](#)). After a few minutes the primordial nucleosynthesis left the universe in a state where the baryonic matter was composed of 75.33%¹ hydrogen, 24.67% helium and traces of deuterium, tritium and lithium ([Planck Collaboration et al. 2016](#)).

Over the years this gas cooled down and gravitationally accreted into molecular clouds and formed stars. The first generations of stars (Population III) fused this gas to heavier elements (metals) and supernovae distributed them into space as a foundation for the formation of new stars of low and high metallicity (Population II and I). Likewise, supernovae of these stars constantly enriched the interstellar medium with metals. Now, the interstellar medium in the Milky Way consists of about 32% helium and traces of other metals ([Danziger 1970](#)).

Our Sun, a metal-rich Population I yellow dwarf star, emerged 4.6 billion years ago ([Bahcall et al. 1995](#)) from an accretion disk formed by a collapsing rotating cloud. The compression within its center resulted in high temperatures which initiated the fusion of hydrogen to helium (primarily pp chain reaction). The fusion reactions produce huge amounts of energy and heat the solar center to a temperature of 15.7 million kelvins ([Christensen-Dalsgaard et al. 1996](#)). The generated energy is transported through the solar body to its surface and eventually into space. The core region extends to about 0.25 solar radii (R_\odot), where the declining temperature becomes insufficient for fusion reactions. The energy transport is dominated by thermal radiation until, because of declining ionization and density, at $0.71 R_\odot$ up to the surface convective motion takes over ([Christensen-Dalsgaard et al. 1991](#)).

The temperature at this transition region (tachocline) is about 2 million kelvins and decreases up to the solar surface to between 4400–6600 K (cite?). Here at the photosphere, the energy is radiated away with an effective black body temperature of 5772 K ([Mamajek et al. 2015](#)), classifying the Sun as a spectral type G2V star. At this surface layer granules, the tops of convection cells, and temporary sunspots are visible. Strong magnetic flux inhibits the convection at sunspots, leading to lower temperature and brightness (for more details on sunspots see the next section 2.2). [Figure 2.1](#) illustrates these photospheric features along with the inner solar structure.

Above the photosphere at the base of the chromosphere the temperature declines to its solar minimum of 3800 K until it raises to 1–3 million kelvins in the corona ([Billings 1959](#)). Up to now it is not fully understood why the corona is so much hotter than the underlying chromosphere—this question is known as the coronal heating problem. The energy transfer mechanisms of choice are magnetic reconnections, wave heating and type II spicules or a combination of these (cite?).

The chromosphere is a 2000 km thick region whose features (numerous spicules, filaments and prominences) can range far into the corona. They consist of by the solar magnetic field channeled chromospheric material, which is enveloped by a thin transition region where the temperature jumps up from ?20 000–35 000 K to coronal temperatures (cite?). Reconnection of magnetic field lines can result in

¹Percentages by mass.

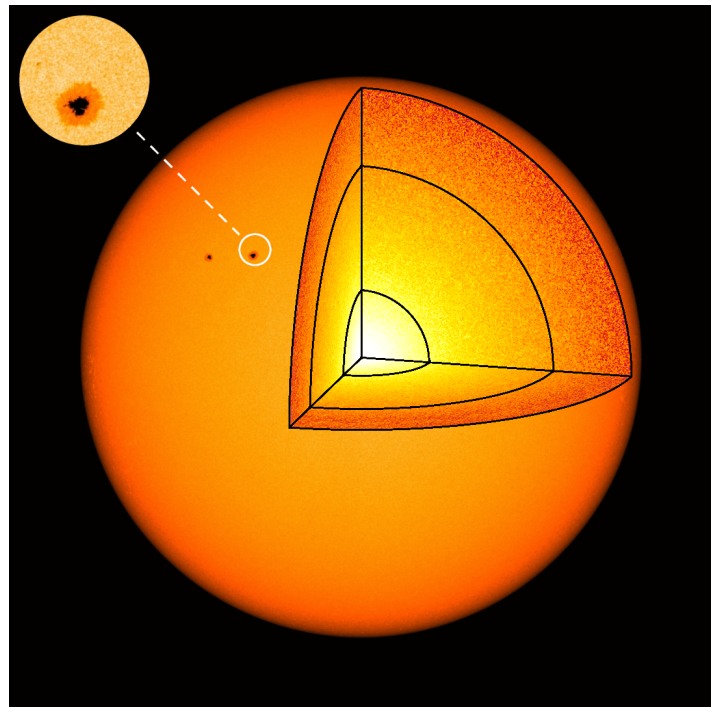


Figure 2.1 Image of the photosphere together with a schema of the solar interior structure. The inset shows the granular surface with a sunspot. The figure is based on a SDO/HMI continuum image from 20 March 2016, credit: NASA/SDO and the AIA, EVE and HMI science teams.

the eruption of filaments into the corona and beyond, termed coronal mass ejections (CMEs) (see also Section XX...). Details of chromospheric features are shown in [Figure 2.2](#).

The Sun's atmosphere is dominated by the varying small- and large-scale solar magnetic field configuration. There are regions where the magnetic field lines arc back to the surface and regions with open field lines. In the latter areas the coronal plasma can—guided by the field—escape into space. Thus these coronal areas are less dense, cooler and therefore appear darker in extreme ultraviolet (EUV) and are called coronal holes (more in Section XX...). In [Figure 2.2](#) a coronal hole is located at the solar south pole.

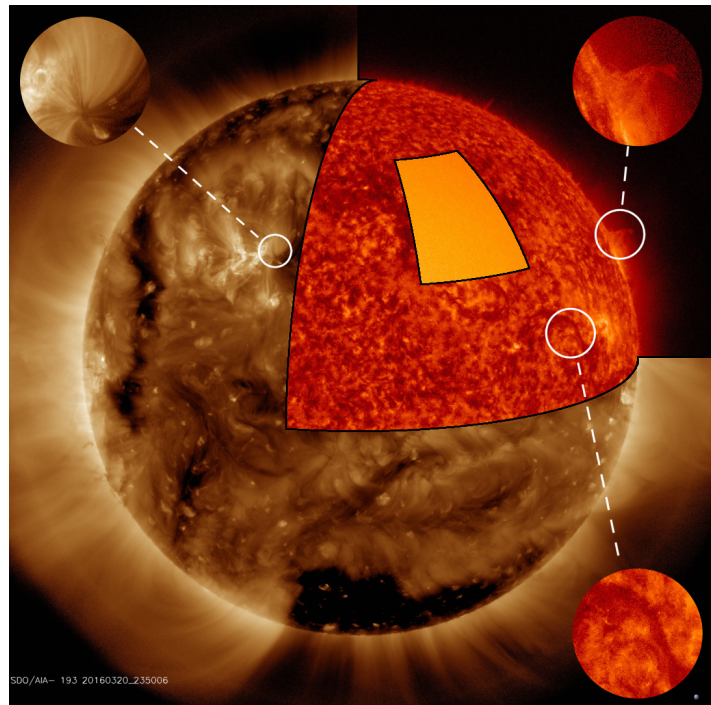


Figure 2.2 Composite image of the solar atmosphere and some of its features. Corona, chromosphere and photosphere are seen in wavelengths of 193 Å, 304 Å and continuum. On the northern limb chromospheric spicules are visible. The enlargements on the right show a prominence and a filament. The dark region at the south pole is a coronal hole. The left inset shows details of the active region belonging to the sunspots in [Figure 2.1](#). The figure is based on SDO/AIA images from 20 March 2016, credit: NASA/SDO and the AIA, EVE and HMI science teams.

From Earth the faint corona and chromosphere can only be observed during eclipses, because of the brightness of the solar disk. There are three effects contributing to the visibility of the corona, photon scattering off free electrons and dust particles, and ion spectral emission lines (termed K-, F-

and E-corona). The image of a solar eclipse reveals the by the magnetic field shaped coronal plasma and features of the red chromosphere, pictured in Figure 2.3.



Figure 2.3 Total solar eclipse image of the inner corona up to 5 solar radii. The picture was taken in Mongolia, 1 August 2008 and is processed from multiple images. Visible are the for a quiet Sun in cycle minimum typical magnetic field's dipole structure and the equatorial streamer belt. Credit: Miloslav Druckmüller, Peter Aniol, Jan Sládeček, 2008. get permission and preferred citation style... into acknowledgments? <http://www.zam.fme.vutbr.cz/~druck/Eclipse/>

Because of the high coronal temperatures, plasma escapes from the solar gravitational field (Parker 1958) with velocities of $200\text{--}800 \text{ km s}^{-1}$. Its acceleration is linked to the coronal heating, but the exact location and process remain an open question (cite?). At a distance of a few solar radii ($\approx 4\text{--}20$) the magnetic field becomes too weak to guide the coronal plasma. From this source surface the solar wind flows radially outward into space until it reaches the termination shock, spanning the heliosphere. Eventually it collides with the local interstellar medium, creating the heliopause. The heliosphere is expected to be a bubble of teardrop shape (and may be led by a bow shock), caused by the Sun's relative velocity of 23 km s^{-1} to the local interstellar medium (Owens & Forsyth 2013). Measurements of the Voyager 1 and 2 spacecraft indicate their passage of the termination shock at about 94 au and 84 au, entering the heliosheath region (Owens & Forsyth 2013). Gurnett et al. (2013) report that in 2012 Voyager 1 actually crossed the heliopause into interstellar space at a solar distance of 121 au. Figure 2.4 illustrates the heliosphere and its surrounding flow structure.

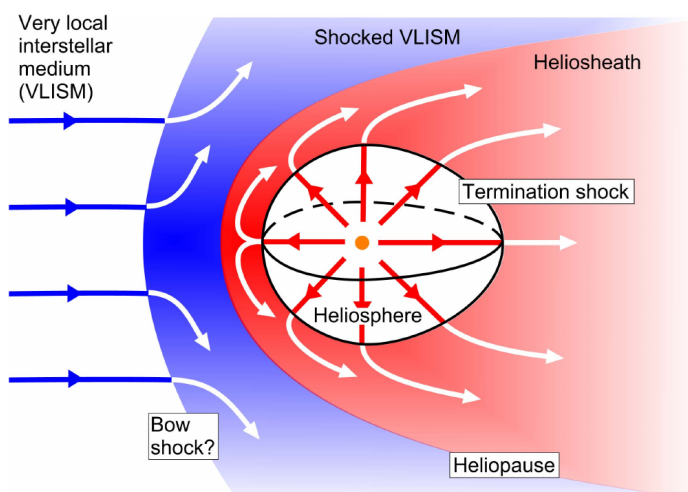


Figure 2.4 Schema of the heliosphere and its surrounding flow structure. The heliosphere is formed by the interaction of the solar wind with the local interstellar medium at the heliopause. (Owens & Forsyth 2013, Fig. 9) get permission...

On its way outwards through the solar system the solar wind, carrying the solar magnetic field, interacts with the planets, their magnetic fields and other solar system bodies. These interactions have various effects, for instance disturbances in planetary magnetic fields with appearance of aurorae and enhanced radiation, atmospheric losses and stripping of cometary tails. Some of these effects can have disruptive consequences for humans and their technology. The topic of space weather effects is further addressed in section 2.6. The magnitude of these effects highly depend on spatial and temporal variations in the solar wind which are rooted in the dynamics of the solar magnetic field.

2.2 Solar dynamics

The spin conservation of the contracting molecular cloud led to a rotation of the Sun with a current average period of about 25 days. The radial convective motion within the solar interior above the tachocline leads to a transport of momentum away from the rotation axis and therefore to a slower polar and faster equatorial rotation in the convection zone (Miesch 2005). This differential rotation is visible on the surface and was first discovered from sunspot observations. With a rotation period of about 34 days the poles have a lag of almost 9 days (for further information on solar rotation see appendix section A.5). The differential rotation in the solar interior can be inferred from helioseismological observations, as seen in Figure 2.5.

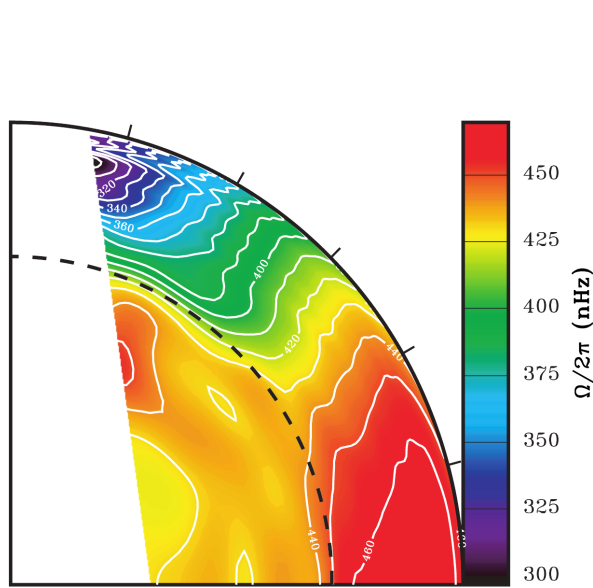


Figure 2.5 Angular rotation velocity in the solar interior. The radiation zone has a nearly solid rotation. Above the tachocline (dashed line) begins the differential rotation of the convection zone. The angular velocity is inferred from helioseismology via observations from the Michelson Doppler Imager (MDI) at the Solar and Heliospheric Observatory (SOHO) spacecraft. (Thompson et al. 2003, Fig. 3) get permission...

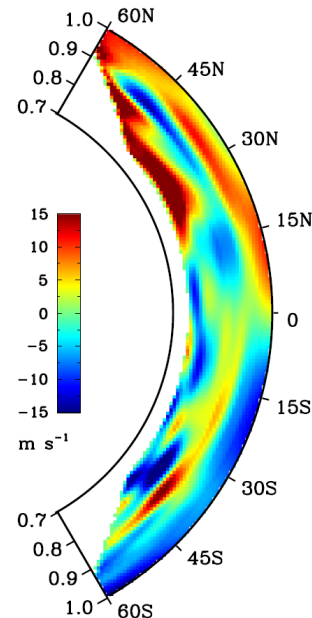


Figure 2.6 Meridional flow velocity profile in part of the convection zone. Positive values are directed towards north. The velocity is inferred from helioseismology via observations from the Helioseismic Magnetic Imager (HMI) at the Solar Dynamics Observatory (SDO) spacecraft. (Zhao et al. 2013, Fig. 4a) get permission...

The resulting large rotational shear at the tachocline generates toroidal magnetic flux (Ω -effect?), which convectively raises to the surface forming sunspots. This solar dynamo is thought to create the major part of the solar magnetic field (Miesch 2005).

$\alpha\Omega$ -dynamo

“Magnetic layer at the base of the convection zone; existence of a deep-seated layer in the Sun with strong toroidal magnetic fields; stronger magnetic fields can be stored for sufficiently long times in the stably stratified region below the convection zone; toroidal magnetic field has an intensity of the order $B \approx 1\text{--}10$ T; the generation of strong toroidal magnetic fields near the bottom of the convection zone;” (Ossendrijver 2003)

Helioseismic measurements reveal that the large-scale convective flow is agglomerated into large convection cells with slow meridional flows of a few m s^{-1} . A poleward subsurface flow and equatorward backflow beneath is detected within each hemisphere, see Figure 2.6.

[The cells have a convection cycle of about 22 years (cite...). As the magnetic field is carried by the

plasma, it emerges at the surface with the same periodicity.]

Within one period the surface magnetic field configuration changes from a dipole structure to a reversed dipole structure with opposite polarity, thus the transition time from one dipole state to the next lasts about 11 years.

In the transition phase toroidal magnetic flux emerges in belts above and below the solar equator manifesting as active regions, resulting in a multipolar structured magnetic field.

bipolar active regions are toroidal magnetic flux, which has emerged as a loop from below the photosphere (magnetic flux ropes). (see [Figure 2.7](#))

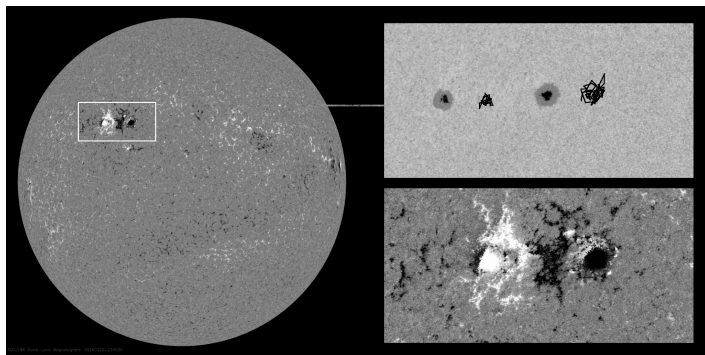


Figure 2.7 Continuum image of both sunspots from [Figure 2.1](#), magnetogram of the same region and of the whole solar disk. A magnetogram shows the polarity of the radial magnetic field component at the photosphere (black/white: xxward/xxward). The highly concentrated magnetic flux at the sunspots is clearly visible in the magnetogram as well as the extended bipolar magnetic field structure of the whole active region (black/white). The figure is based on SDO/HMI continuum and magnetogram images from 20 March 2016, credit: NASA/SDO and the AIA, EVE and HMI science teams. switch sides...

poloidal field + diff. rot. \Rightarrow toroidal field (Ω -effect) Miesch2005 p. 18 + p. 31
switching between states of strong poloidal and toroidal field

- the solar dynamo: (toroidal to poloidal field)
- turbulent plasma motions from convective flows generate disorganized magnetic fields
- differential shear at tachocline amplifies fields to strong coherent toroidal flux (Ω -effect); magnetic layer located at the base of the convection zone
- stronger flux ropes raise to surface (buoyantly)
- Coriolis force twists them systematically, stronger at higher latitudes
- twisted tubes emerge on the surface as bipolar active regions
- amplification of mean fields by fluctuating motions (α -effect) and turbulent diffusion create large-scale poloidal field

Since regions of strong magnetic flux are visible as sunspots on the photosphere, they were known well before the common era by Chinese and Greek scholars. Systematic sunspot observations exist since 1610, shortly after the invention of the telescope (cite?). In 1843 Schwabe discovered the 11-year periodicity in the sunspot occurrence (cite?). To record solar cycles in 1848 Wolf (et al?) introduced the sunspot number (SSN) and cycle number (with the zeroth occurring in 1749) (cite?), see [Figure 2.8](#).

The large variations in cycle length (9–14 years) and intensity (0–350 SS_n) make it difficult to predict the course of the next solar cycle (cite...).

long-time variations like the Maunder minimum... see Hathaway2015

Observations of the surface radial magnetic field show the appearance of bipolar magnetic flux at belts of about $\pm 20^\circ$ latitude at the beginning of a cycle and a shift towards lower latitudes at the end of a cycle (magnetogram figure of sunspot?). Thus the plot of surface magnetic field over latitude and time reveals a butterfly pattern. The emerging flux (its polarity alternates with each cycle) is carried by the slow meridional surface flow poleward, resulting in the polar field switch, see [Figure 2.9](#). The ordered dipole structure in solar cycle minimum leads to open polar field regions with large coronal

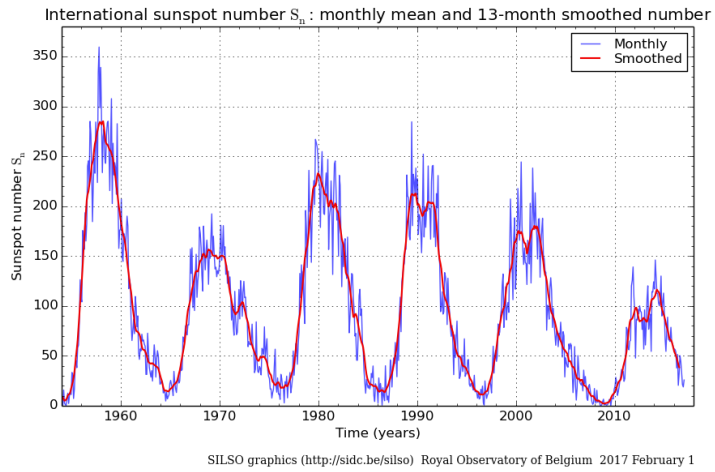


Figure 2.8 Monthly mean sunspot number (blue) and 13-month smoothed monthly sunspot number (red) since 1954. Credit: SILSO data/image, Royal Observatory of Belgium, Brussels, 2017-02-01. get permission... Update this figure before printing!!!

holes and a closed equatorial field belt/streamer belt (clearly visible in Figure 2.3).

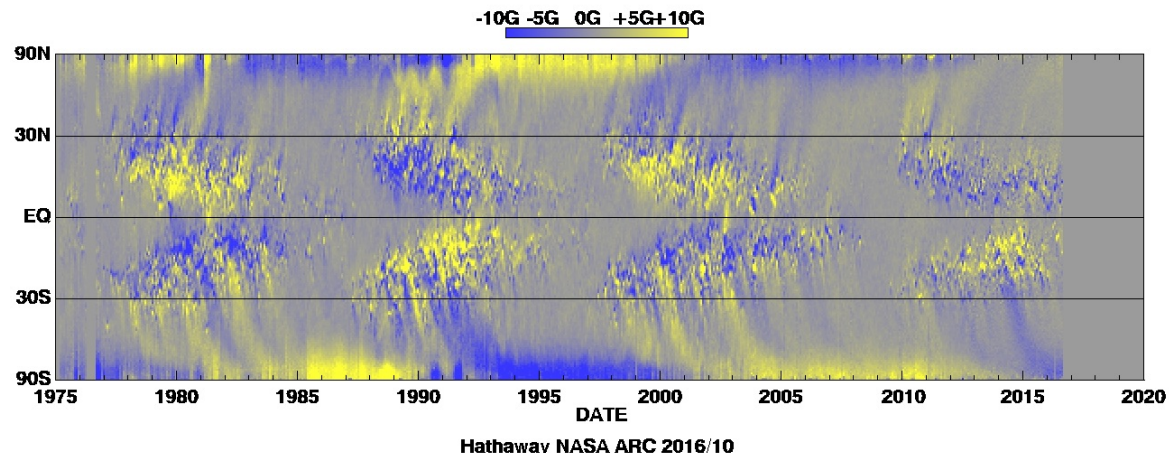


Figure 2.9 Magnetic butterfly diagram of the synoptic radial magnetic field on the solar surface. Yellow represents an outward directed magnetic field (positive), blue inward (negative). The data is obtained from instruments on Kitt Peak National Observatory and from the MDI at the SOHO spacecraft. Credit: David Hathaway, NASA Marshall Space Flight Center; see also [Hathaway \(2015, Fig. 17\)](#). Update this figure before printing! get permission...

sunspot butterfly pattern ([Maunder 1904](#))

sunspots NE active regions; active regions forming streamer belt?

The magnetic field geometry during cycle maximum is more complex, due to the in mid-latitudes emerging flux, which is related to the then stronger toroidal component of the solar magnetic field.

HMF with figures DQCS + Parker spiral

This leads to the chaotic appearance of closed field lines even at higher latitudes/poles and coronal holes covering equatorial regions. tbm

sw in minimum: streamer belt and polar HSSs

fast solar wind emerges from CHs

slow from closed field streamers

This is confirmed by the Ulysses spacecraft, which measured the solar wind speed in a polar orbit covering more than one solar cycle (Figure 2.10).

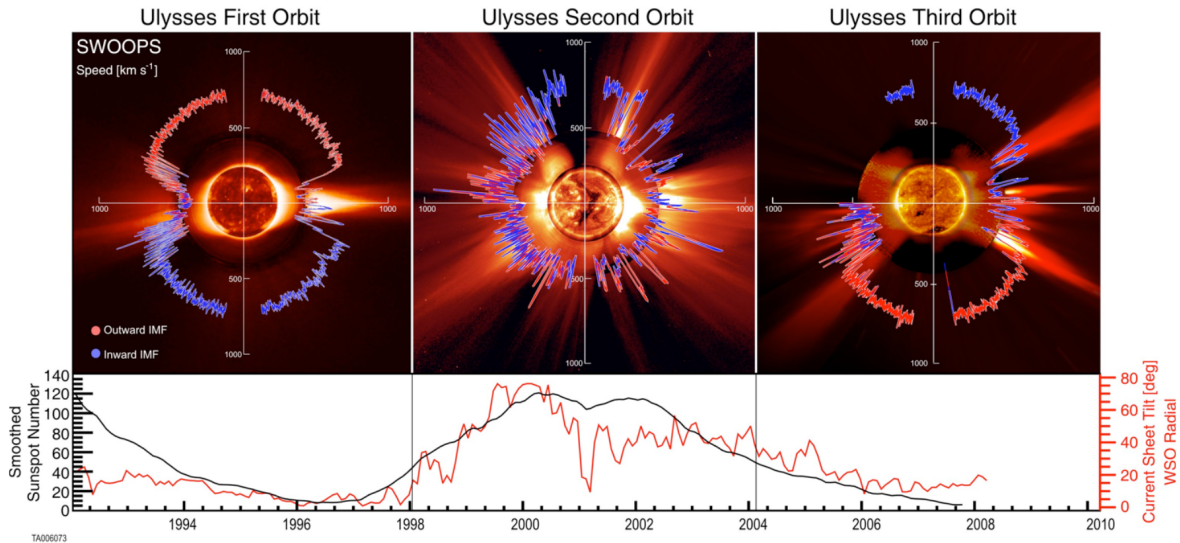


Figure 2.10 Solar wind velocity and magnetic field polarity over latitude during low and high solar activity for the three orbits of the Ulysses spacecraft. The SSN and CS tilt angle are plotted as well. (McComas et al. 2008, Fig. 1). ask for high res. image and permission...

keywords:

SSN -> magnetic surface activity (butterfly diagram) => poloidal/toroidal field -> min/max polar CHs (quiet/active Sun figure) -> HMF (quiet B-field figure) -> quiet HMF Parker spiral (figure) -> solar wind -> slow/fast sw pattern (Ulysses figure))

solar wind plasma composition and properties -> visible solar wind structures (coronagraph image; with CME and streamer) -> stream interface (figure) -> in situ measurements (example in situ CIR/HSS plot)

stream interfaces (figure and link to previous CIR plot) -> HCS/HPS

CMEs (link to previous coronagraph image; in situ CME/MC plot; CME schema figure?)

differential rotation/shear at tachocline -> B-field
meridional flow -> solar cycle period
dipole structure, open and closed field lines
polar coronal holes
streamer/equatorial streamer belt
solar wind

open field lines (coronal holes) -> HSSs
equatorial ballerina model -> CIRs (figure?)

The solar differential rotation wraps the magnetic field lines, accumulating tension, leading eventually to relief with a magnetic reconfiguration by field line reconnections.
-> release of much energy -> flares, CMEs

solar wind's impact on Earth

the rotation axis is tilted from the normal of the ecliptic by $i_{\odot} = 7.25^\circ$ (U.S. Nautical Almanac Office 2015) (refer to or put into appendix??).

2.3 Solar wind

see Kivelson1995, p14+91

first observed at solar eclipses?, before? deduced by Parker from theory/Carrington from geomagnetic storms?

discovered via eclipses?

see eclipse photo from Druckmüller [Figure 2.3](#)

in 1958 Parker predicted/postulated the solar wind ([Parker 1958](#))

expanding isothermal atmosphere (solar wind model)

continuous supersonic radial outflow of plasma

-> also Parker spiral of HMF (see [Figure 2.12](#))

2.4 Heliospheric magnetic field

reviews: [Balogh & Jokipii \(2009\)](#) (for heliosheath), [Owens & Forsyth \(2013\)](#)

Winterhalter1994 The heliospheric plasma sheet:

"the narrow heliospheric current sheet (ca. 3000–10000 km thick), together with the heliospheric plasma sheet in which it is embedded. The heliospheric plasma sheet region is identified by a significantly enhanced plasma beta caused by density enhancements and diminished magnetic field strength and is about 20 to 30 times the thickness of the current sheet."

heliospheric current sheet (HCS)

heliospheric plasma sheet (HPS)

ballerina model... (search figure...)

Photosphere: magnetic bright points (MBP) 1–2 kG

their convective motion result in wavelike fluctuations of the thin tubes

low chromosphere: thin flux tubes expand laterally and merge to a homogeneous network field

below the chromosphere-corona transition region: the network magnetic field expands laterally and merges again to a large-scale canopy (image)

[above the Alfvén critical point—where the wind speed equals the local Alfvén speed at about $10 R_{\odot}$ —both the inward and outward modes are advected (advect: convect horizontally) outward with the wind

superradially expanding magnetic flux tube

([Cranmer & van Ballegooijen 2005](#))]

see also paper citations...

analytical solar magnetic field model for solar minimum conditions ([Banaszkiewicz et al. 1998](#))

dipole plus quadrupole plus current sheet (DQCS) solar magnetic field model

The DQCS model with its quadrupole part having a direct link from the solar equator to infinity along the equatorial plane and current sheet. (see [Figure 2.11](#)) ([Banaszkiewicz et al. 1998](#))

compare with field geometry from eclipse [Figure 2.3](#)...

Parker spiral, source surface and HCS, see [Figure 2.12](#)

MHD simulations based on Voyager 1 and 2 measurements within the heliosheath indicate the formation of magnetic bubbles (reconnected sector regions) at the sector boundary caused by the compression before the heliopause, flowing away to the heliosheath tail ([Opher et al. 2011](#)).

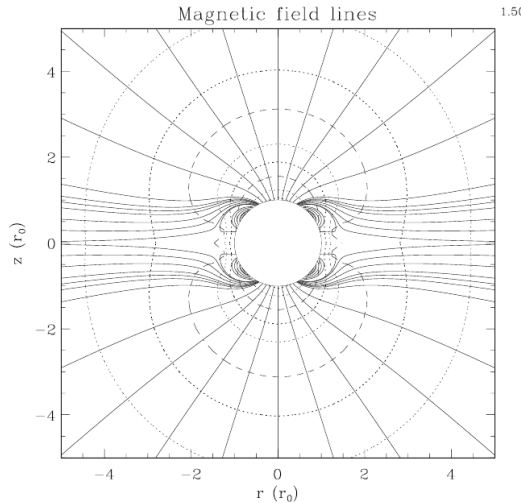


Figure 2.11 Solar magnetic field geometry from the DQCS model with field lines (solid) and constant field strength surfaces (dashed). The quadrupole part allows equatorial outflows along the current sheet. (Banaszkiewicz et al. 1998, Fig. 3) get permission...

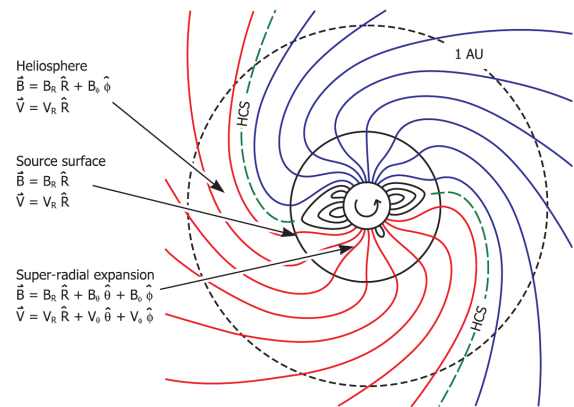


Figure 2.12 Illustration of the solar magnetic field Parker spiral formation by rotation of the solar wind source surface. Between solar wind flows of opposite magnetic field polarity a heliospheric current sheet (HCS) forms. (Owens & Forsyth (2013, Fig. 1), adapted from Schatten et al. (1969, Fig. 1)) get permission...

2.5 Solar wind properties and structures

list event/structure types

solar wind structures source regions: sunspots/active regions, coronal holes, filaments

sw density considerations, see presi S³

2.5.1 Solar wind plasma

Plasma in general (properties (H/He/metal composition; see paper...), Plasma-beta, etc.)
solar wind properties, slow/fast wind, MHD waves (Alfvén waves)

special events/configurations, which can appear (CIRs, HCS/HPS, etc.) HSS, sector boundaries, CIRs, CMEs

2.5.2 Slow solar wind

regions with closed lines

trapped plasma, slow solar wind from streamers

2.5.3 High speed streams

regions with open lines

coronal holes as sources of fast sw

sw plot of HSS with CIR to refer to

Schwenn (1983): “During the Skylab era in 1973/74 we learned that these high speed streams emerge from coronal holes (Hundhausen, 1977 and references therein).”

2.5.4 Stream interaction regions

Streams of fast wind catch slow wind
-> compressions, shocks, deflections

Corotating interaction regions (CIRs)
Stream interaction regions (SIRs)

formation of stream interface and stream deflection, see Figure 2.13
refer to sw figure of CIR

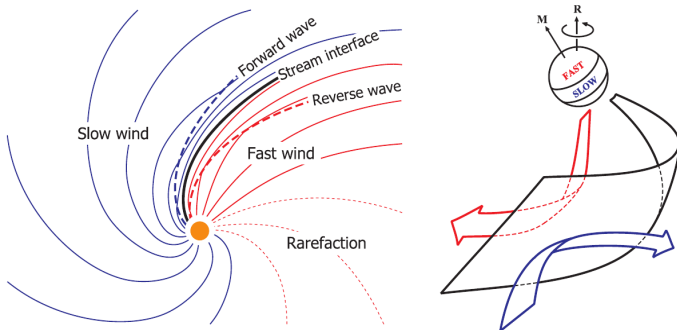


Figure 2.13 Schema of the formation of a stream interface (left) and deflection of streams (right), both generated from interactions between slow and fast solar wind. (Owens & Forsyth (2013, Fig. 7); right panel adapted from Pizzo (1991, Fig. 2))
get permission...

2.5.5 HCS / HPS

from sector boundaries (ballerina skirt)

2.5.6 Coronal mass ejections

Coronal mass ejections (CMEs) (discovery (Carrington), definition (Hundhausen?), models, GCS (conception of 3-dim CME shape -> enables Earth arrival time forecast from modeled direction and velocity))

active regions:
sunspots, magnetic reconnections, flares, post-eruptive arcades

coronagraph figure of CME (COR2 image, SECCHI/STEREO)
in situ solar wind figure of same CME (recent one from 2016)

CME-plasma properties
+ flares and SEPs often accompany CMEs

Magnetic clouds

magnetic cloud (MC); refer to in situ plot
See BS magnetic cloud model in analyses methods chapter MVA...

2.6 Space weather

Solar wind influences the Earth's magnetosphere and can disturb sensitive technical systems
understanding its properties helps with prediction of events

influences on human infrastructure/technical systems

various space weather effects, for instance disturbances in magnetic fields, aurorae, episodes of enhanced radiation, atmospheric losses and stripping of cometary tails. figures of these effects?

reference to [Bothmer & Daglis \(2007\)](#), maybe images

2.6.1 Solar influence on Earth

Carrington made first connection between terrestrial magnetic field and solar flares. correct?

there are several types of solar-terrestrial relations, [Bartels \(1962\)](#) listed:

- a) irregular flare and CME effects (Carrington)
- b) 11-year solar cycle effects
- c) 27-day solar rotation effects
- d) daily effects (x-ray and light)

seasonal effects from Earth orbital distance, inclination (solar rotation axis angle) and Earth tilt (see [Figure 2.14](#))

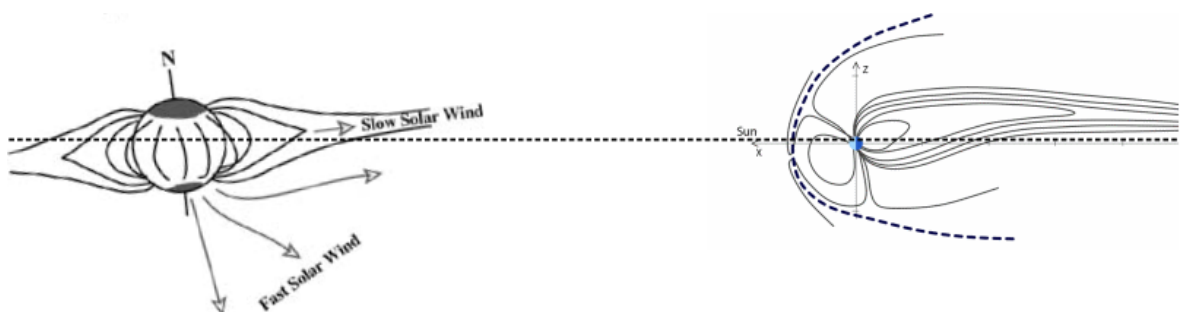


Figure 2.14 Sun-Earth geometry in the plane orthogonal to the ecliptic (not to scale); Solar magnetic field-magnetosphere geometry. Seasonal effects are: solar tilt, Earth distance and Earth tilt

solar wind and its species
solar radiation
solar energetic particles (SEPs)
gravitation

magnetosphere
ionosphere?
aurorae
geomagnetic storms (several days, from CMEs)
substorms (few hours, from CIRs??)

for humans and their technology important effects: enhanced radiation, geomagnetic storms
lovely, disruptive, dangerous consequences <- read in VBbook

at Earth the solar wind total energy flux (1.45 mW/m^2) is only about one millionth of the solar radiation flux (see [Schwenn \(1990, p. 153\)](#))

"The principal users affected by geomagnetic storms are the electrical power grid, spacecraft operations, users of radio signals that reflect off of or pass through the ionosphere, and observers of the aurora." NOAA cite

2.6.2 Magnetosphere

shape formed by dynamic pressure..., similar to heliosphere in ISM...

2. Basics

bow shock, magnetotail, magnetosheath, magnetopause
add ecliptic and terrestrial tilt angle; with plasmoid?
see Figure 2.15

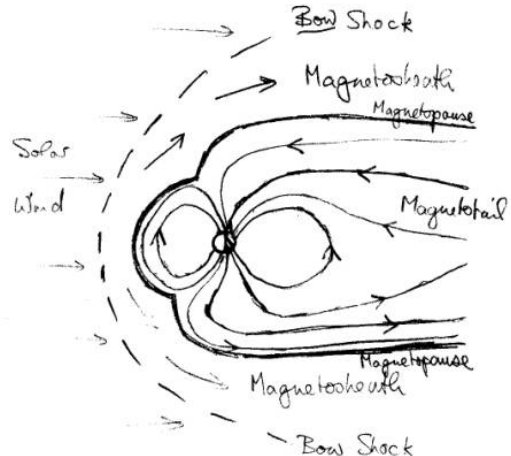


Figure 2.15 temp figure “The cavity is called the magnetosphere. It has a relatively well-defined outer boundary, the magnetopause.”

turbulence with sw (KH or RT instabilities), see subsection 2.6.4

Earth magnetic field strength at a height of 36 000 km (geostationary): 100 nT
Earth magnetic field strength at the surface - equator: 30 000 nT - poles: 60 000 nT (cite?)

magnetopause = current layer??

two extreme cases of Bz orientation: parallel/antiparallel compression/reconnection (see Figure 2.16)

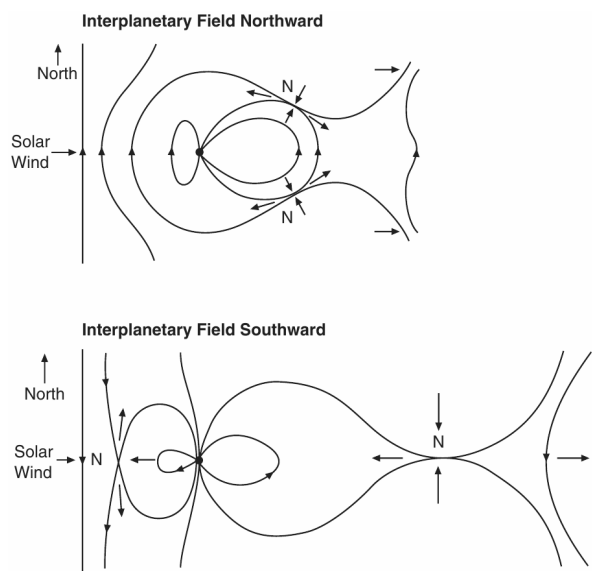


Figure 2.16 reconnection and compression depending on the interplanetary magnetic field orientation; figure 4.8 from Bothmer & Schwenn (1998, p. 116), adapted from Dungey 1961, 1963. accelerated flows are arrowed; N points are X points...

standoff distance: (Bothmer & Daglis 2007, p. 112)

$$d = \frac{107.4}{1R_E} (NV^2)^{-1/6} \quad (2.1)$$

Even in “ancient” times (when?) a correlation between solar particles and disturbances in the magnetosphere were known of (Bartels 1962).

magnetosphere variations due to solar wind
 magnetosphere protects from radiation (maybe from solar wind stripping atmosphere away?)

effects: aurorae, ...

ring current systems

definition of:
 magnetic storm...
 substorm...

subsection Ionosphere?
 its variations due to solar radiation (day/night cycle and flares)
 ionosphere -> TEC -> GNSS error

2.6.3 Geomagnetic indices

Geomagnetic observatories are distributed widely over the globe, measuring the local magnetic field at their position. Several sets of stations, covering specific regions, are defined to monitor the state of different parts of the magnetospheric system. Magnetic measurements from these sets define several geomagnetic indices. The International Association of Geomagnetism and Aeronomy (IAGA) supports the following global geomagnetic indices which are serviced by the International Service of Geomagnetic Indices (ISGI)²: The *aa* index is designed to represent the amplitude of the global geomagnetic activity, normalized to a geomagnetic latitude of $\pm 50^\circ$. The *am* index characterizes the global geomagnetic activity. The *Kp* index is designed to measure geomagnetic disturbances from solar particle radiation [reword...]. The *Kp* index is described in more detail in subsection 3.2.2. The *Dst* index monitors the intensity of the magnetospheric ring current. The *PC* index monitors the polar cap magnetic activity – it approximates the amount of energy which entered the magnetosphere through solar wind coupling. The *AE* index and its relatives *AU*, *AL* and *AO* measure the magnetic effects of the northern auroral electrojet. The first three listed indices (*aa*, *am* and *Kp*) are calculated from different sets of local 3-hourly *K* indices, which measure the local magnetic disturbances at the observatories. There exist several more indices that are based on some of those listed above.

[for *Kp*, *AA* and *Dst* read Section 7.4 in book Bothmer & Daglis (2007)...
Dst (read book Jursa1985 p. 4-31)]

2.6.4 Solar wind–magnetosphere coupling

E-field:

$$\mathbf{E}_{\text{IMF?}} = -\mathbf{V} \times \mathbf{B}_{\text{IMF}} \quad (2.2)$$

...derive from Lorentz force

(Because of high plasma conductivity the E-field is not existent.)

Axford1964 viscous interaction (of turbulent nature, KH/RT instabilities, KH instabilities at the flanks of the magnetosphere) is a viable source of drag force/solar storm energy input into magnetosphere

Otto&Nykyri1982 KH instabilities/vortices force magnetic reconnection even at northern IMF and are able to account for observed mass flux

Newell et al. (2007) and Newell et al. (2008): coupling consists of merging and viscous part (reconnection and turbulence)
 merging part: rate magnetic flux is opened at the magnetopause

²ISGI website: <http://isgi.unistra.fr/>

[2. Basics](#)

viscous part: reconnection due to Kelvin-Helmholtz instabilities at the boundary

Merkin2013 MHD simulation of velocity shear at magnetosphere boundary with northern IMF; KH instabilities; double-vortex sheet structure

3 Data

3.1 Instruments

For analyzing the solar wind and related effects on the Sun there are remote instruments (solar imager and coronagraphs) and in situ instruments (magnetometer and plasma detector).

Here the basic principles of the latter are described, because the analyses performed in this thesis are based on in situ solar wind measurements.

3.1.1 Magnetometer

Spacecraft nowadays carry two different magnetometer types, one for measuring the magnetic field direction and its strength and the other for observing the magnetic flux and detecting waves.

A flux gate magnetometer consists of two coils around a core—one coil with alternating current, which is compared with the induced current signal from the other. Without external magnetic field both patterns match. The core is easier magnetized in direction of an existing external magnetic field, in which case the patterns differ. It measures...

In a search coil magnetometer one coil is placed around a core; measures plasma waves - where?

Because these magnetometer types are directional, they often are placed in two sets of triaxial configurations, attached on booms to minimize the influence of the spacecraft's own magnetic field.
L-> which is generated by surface charges?/electrons?/ionization?/the instruments?

3.1.2 Plasma detector

several spectrometers with different energy ranges

isotope spectrometer - isotopic abundances of SEPs
ionic charge analyzer - charge state of SEPs
sw ion mass spectrometer -
sw ion composition spectrometer -
radio burst tracker

A plasma detector measures the ion energy frequency distribution, which consists basically only of protons and alphas in solar wind (see Figure 3.1). see also subsection 2.5.1

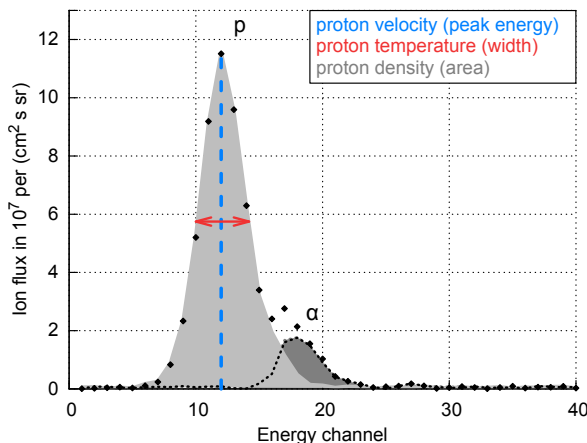


Figure 3.1 Example of an ion energy spectrum with synthetic data. Here proton and helium (alpha) peaks are distinguishable...

3. Data

From the energy spectrum the velocity, density and temperature can be derived.

The bulk velocity is derived from the distribution's average energy.
The number density is the area of the distribution.
The temperature scales with the distribution's width.

3.2 Data sources

Spacecraft / data sets

Positions:

Earth:

imager, magnetosphere

L1 - first Lagrangian point:

ACE (siehe auch space weather spacecraft Liste)

Wind etc. (OMNI)

DSCOVR

1 au orbit

STEREO A and B

inner heliosphere:

Helios 1 & 2

PSP

outer heliosphere:

Voyager 1 and 2

Ulysses

also RT-data sources? Wind, ACE, STEREO A and B, DSCOVR

A time coverage overview of the data sets used in the analyses of this thesis (SSN, K_p index, LRO, HRO, Helios 1 and 2) is plotted in [Figure 3.2](#).

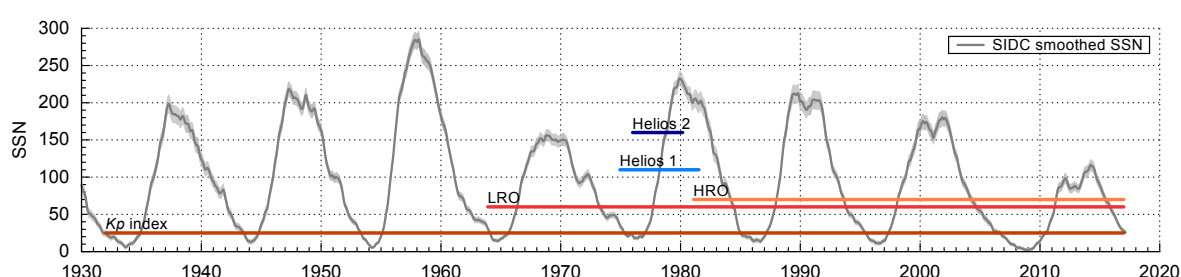


Figure 3.2 Time coverage of the K_p index, low and high resolution OMNI, Helios 1 and Helios 2 data sets until end of 2016. The SIDC 13-month smoothed monthly SSN is plotted in the background.

3.2.1 Sunspot number

SSN history

add SSN figure of history incl. Maunder minimum?

SIDC/SILSO...
WDC-SILSO – World Data Center-Sunspot Index and Long-term Solar Observations

3.2.2 K_p index

Julius Bartels introduced the K index in 1938 and designed it to measure the intensity of geomagnetic disturbances ([Bartels et al. 1939](#)). Its name originates from 'Kennziffer' – the german word for

characteristic digit. The K index is a measure for the maximal variation of the surface magnetic field, observed in a magnetogram within 3-hour intervals. Its scale in the range 0–9 is a quasi-logarithmic representation of the actual magnetic field strength's variations.

The Planetary K index (Kp) is a planetary geomagnetic disturbance index, introduced by Bartels in 1949 at the Institute for Geophysics, University of Göttingen (Bartels & Veldkamp 1949). Kp is the weighted average of 13 K_s indices, which are the standardized versions of the local K indices measured at 13 observatories. These contributing observatories are located around $\pm 50^\circ$ geomagnetic latitude and their distribution is biased towards Europe (see Figure 3.3).

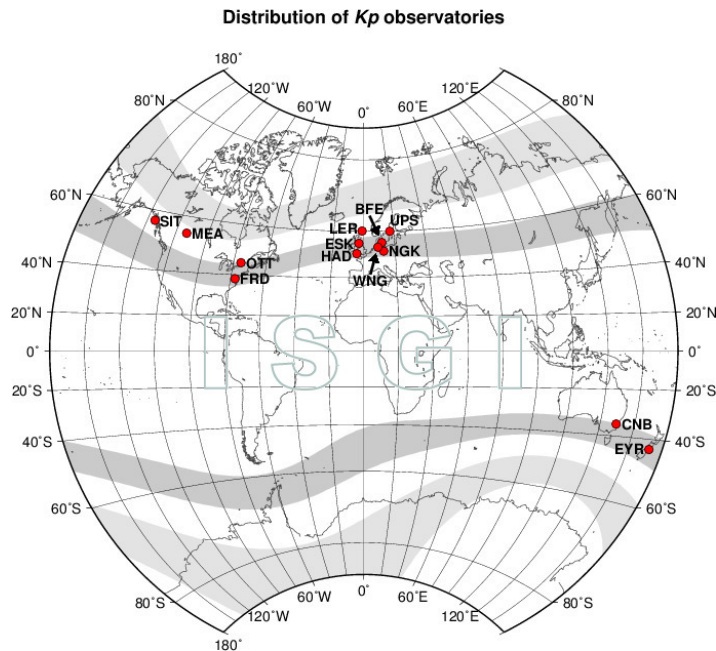


Figure 3.3 Distribution of the 13 K_p observatories. Credit: International Service of Geomagnetic Indices (ISGI), 2013. look into cc license...

To benefit from its higher precision, its scale, in the range 0–9 as well, is further divided into thirds, represented by the suffixes '+', 'o' and '-' (e.g., 3o, 3+, 4-, 4o). The K_p indices are often visualized in musical diagrams, where they are stacked into periods of 27 days to enable the detection of recurrent activities, as seen in Figure 3.4.

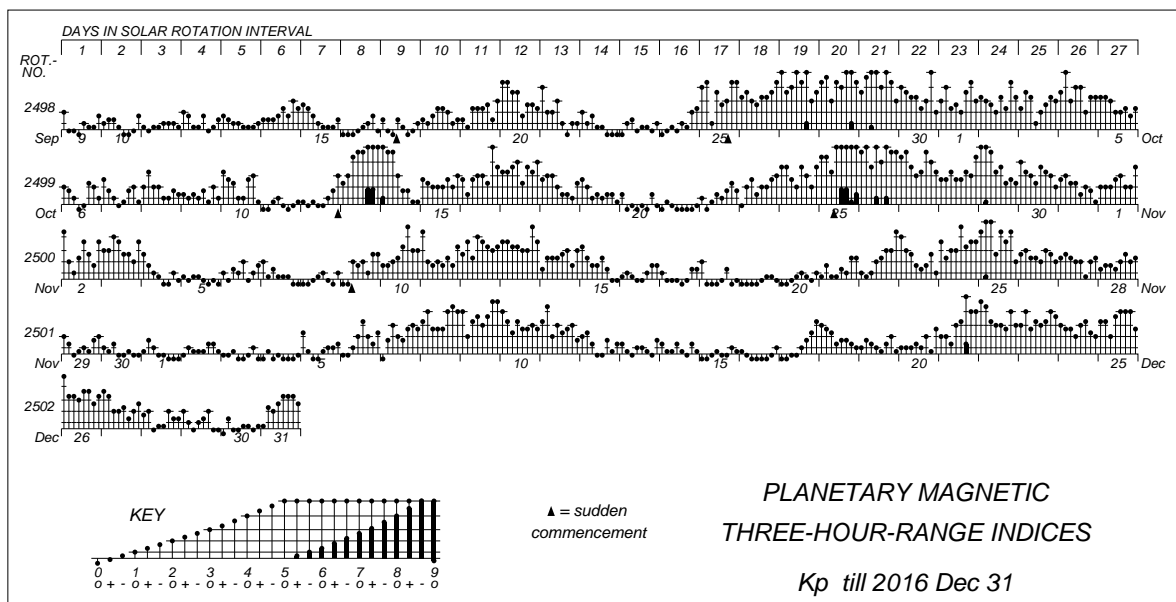


Figure 3.4 Bartels musical K_p diagram for the time period from September until end of December 2016. Two sudden commencements with following geomagnetic storms, having a maximal K_p of 6+, can be seen in October. Credit: GFZ Potsdam, 2017. look into cc license...

3. Data

Table 3.1 Defined table for the conversion from the K_p index to the equivalent ap index, which represents the magnetic field strength in units of 2 nT.

K_p	0o	0+	1-	1o	1+	2-	2o	2+	3-	3o	3+	4-	4o	4+
ap	0	2	3	4	5	6	7	9	12	15	18	22	27	32
K_p	5-	5o	5+	6-	6o	6+	7-	7o	7+	8-	8o	8+	9-	9o
ap	39	48	56	67	80	94	111	132	154	179	207	236	300	400

The K_p index can be converted to the 3-hour equivalent ap index, which represents the magnetic field strength at a surface position of about 50° dipole latitude. The conversion is done via a table defined by Bartels, in which the value of the ap index is scaled in units of 2 nT (see Table 3.1). There are further geomagnetic indices which are derived from the K_p index. They include Ap , the daily ap average, Cp , the daily ap sum mapped via a defined table to the range 0–2.5 and $C9$, a mapping of Cp via a defined table to the range 0–9. The definitions of Q-days (quiet days) and D-days (disturbed days) are also obtained from the K_p index.

The International Association of Geomagnetism and Aeronomy (IAGA) adopted the K_p index in 1954. The K_p index was maintained in Göttingen until January 1997 – now the German Research Centre for Geosciences (GFZ) in Potsdam supplies the K_p index and thereof derived indices. The GFZ provides historical and quicklook data of the indices via their website¹. The data was extended backwards and is available from 1932 onwards.

further uses of the K_p index:
The NOAA G-Scale for geomagnetic storms (G 1 to G 5) is based on the K_p index².
GNSS error, auroral boundary positions

“It is designed to measure solar particle radiation by its magnetic effects.“

3.2.3 OMNI data set

a data set merged from different sources
The OMNI data (King & Papitashvili 2005) were obtained from the GSFC/SPDF OMNIWeb interface.

from spacecraft located near the Lagrange point L1 upstream of Earth
time-shifted to the bow shock of the magnetosphere

OMNI2 H0 MRG1HR (1963-201308) Cite from CDAweb: Hourly near-Earth solar wind magnetic field and plasma data, energetic proton fluxes (> 1 to > 60 MeV), and geomagnetic and solar activity indices.

NASA, Goddard Space Flight Center (GSFC), Space Physics Data Facility (SPDF): <http://spdf.gsfc.nasa.gov/>

- Coordinated Data Analysis Web (CDAWeb): <http://cdaweb.gsfc.nasa.gov/>
- OMNIWeb Plus: <http://omniweb.gsfc.nasa.gov/>

intercalibrated multi-spacecraft solar wind data
Various spacecraft contribute to the interplanetary magnetic field (IMF) and solar wind plasma OMNI data, as seen in Figure 3.5.

Solar Wind Structures

Solar Wind Structures (SWS) list
derived by Richardson.... from OMNI data (only?)
permission received.

¹GFZ website for geomagnetic indices: <http://www.gfz-potsdam.de/de/kp-index/> (existent in 2017-10-29)

²NOAA Space Weather Scales website: <http://www.swpc.noaa.gov/noaa-scales-explanation> (existent in 2017-10-29)

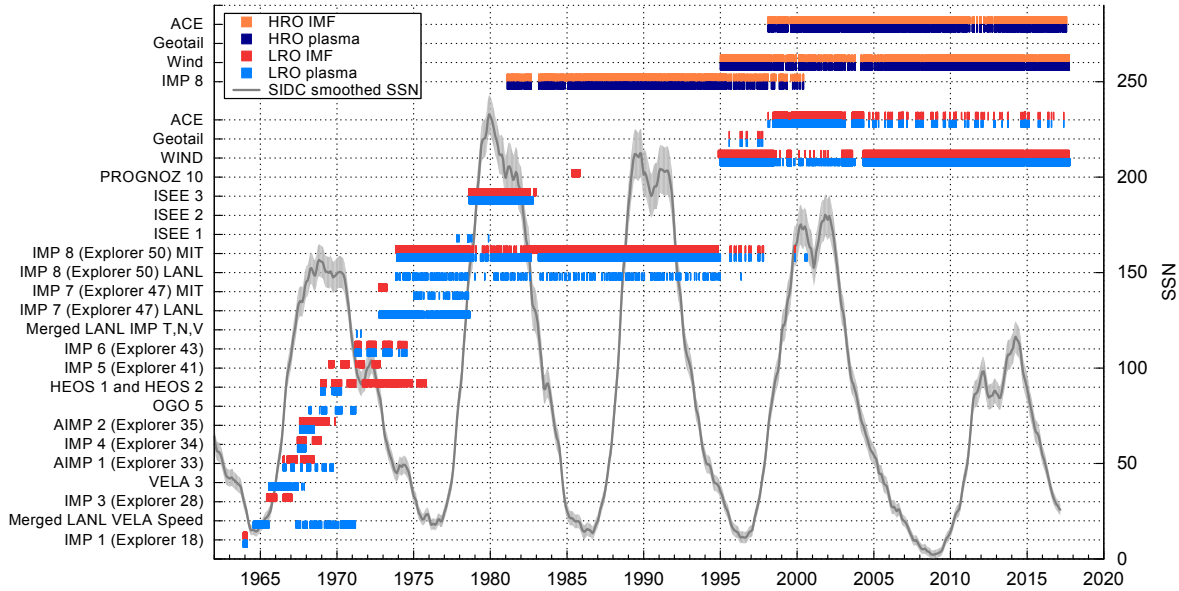


Figure 3.5 IMF and solar wind plasma data source spacecraft for the high and the low resolution OMNI (HRO, LRO) data sets until end of 2016. The SIDC 13-month smoothed monthly SSN is plotted in the background.

characterization of near-Earth solar wind structures since 1963
SWS lists (Richardson et al. 2000) and (Richardson & Cane 2012)

3.2.4 Helios probes

see Helios data readme.txt

see paper

two different fluxgate magnetometers and a search coil magnetometer

see Figure 3.6

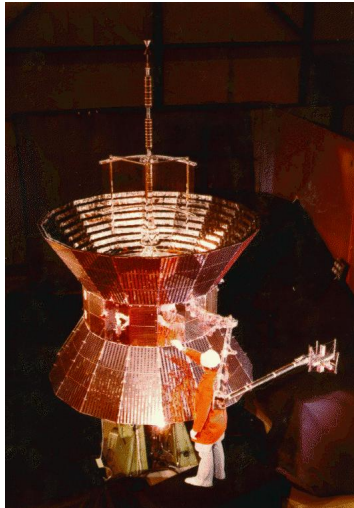


Figure 3.6 One of the nearly identical twin Helios spacecraft. Credit: Max Planck Institute for Solar System Research. get permission...

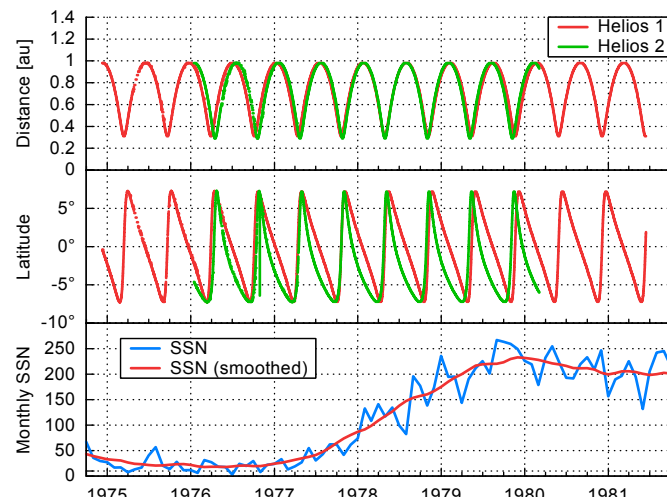


Figure 3.7 Plot of the Helios probes' solar distance and HGI latitude over their mission time, together with the monthly SSN and 13-month smoothed monthly SSN.

solar distance, HGI latitude and sunspot number during the Helios missions; see Figure 3.7

3. Data

Helios orbit in the ecliptic plane and in the latitude polar plane (see Figure 3.8)

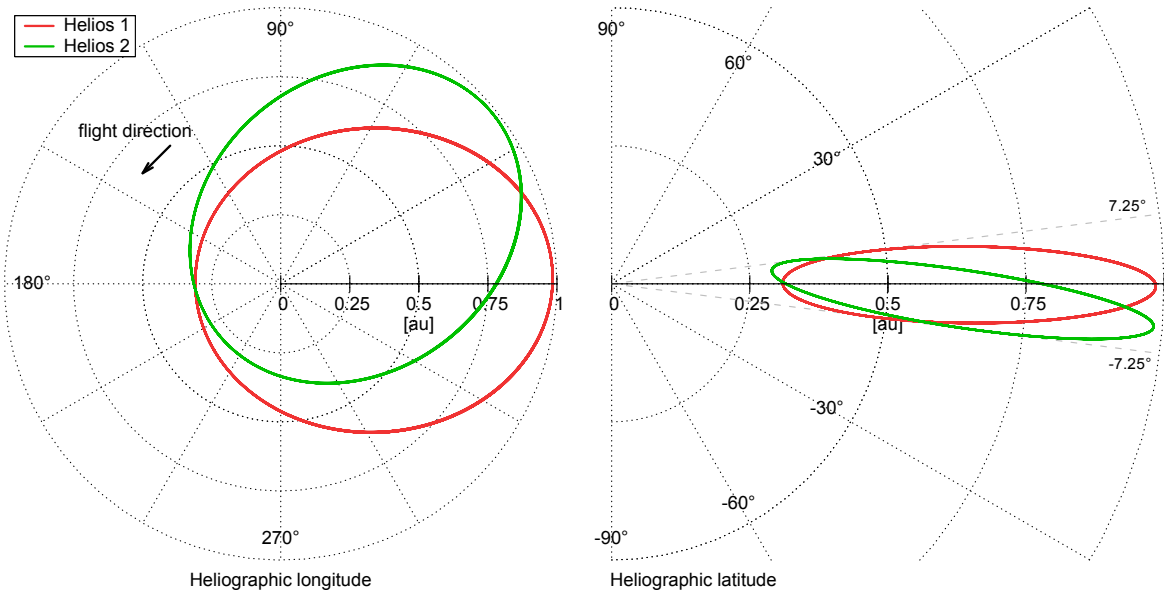


Figure 3.8 Helios orbits in the solar equatorial plane (left) and polar plane (right) (HGI-coordinates). change colors?

The Helios magnetic field and plasma data counts over solar distance are plotted in Figure 3.9 and over latitude are plotted in Figure 3.10. build 2-panel figure...

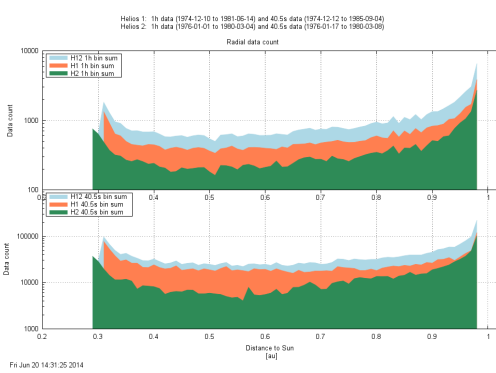


Figure 3.9 Plot of the Helios data count per 0.01 au solar distance bins. plot for mag and plasma individually..., combine with latitude plot...

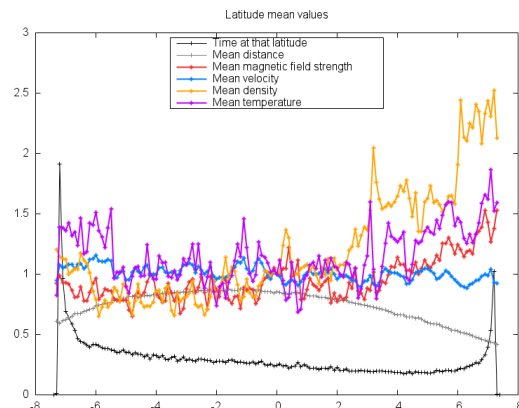


Figure 3.10 Plot of the Helios data count per 0.1° latitude. plot for mag and plasma individually... remove all other curves...

Solar wind data courtesy of R. Schwenn, Max-Planck-Institut für Aeronomie, Lindau, magnetic field data courtesy of F. Neubauer, Universität zu Köln. (see paper; into acknowledgements...)

data sources – see paper for replacing the following data
solar wind parameters: ACE, Helios, OMNI
geomagnetic indices: Kp, OMNI

Space Physics Data Facility (SPDF)

HELIOS 1 and 2 - orbital Parameters
<http://spdf.sci.gsfc.nasa.gov/pub/data/helios/helios1/traj/>

<http://spdf.sci.gsfc.nasa.gov/pub/data/helios/helios2/traj/>

Helios hourly merged mag & plasma data:
HELIOS1_COHO1HR_MERGED_MAG_PLASMA_2965.txt
HELIOS2_COHO1HR_MERGED_MAG_PLASMA_3096.txt
<http://cdaweb.gsfc.nasa.gov>
temporal coverage of merged data
Helios 1: 1974-12-10 - 1981-06-14
Mag data availability: 42.6 %
Plasma & orbit data availability: 76.4 %
Helios 2: 1976-01-01 - 1980-03-04
Mag data availability: 54.4 %
Plasma & orbit data availability: 91.8 %

3.2.5 Parker Solar Probe

Sun angular diameter comparison, see presi S³

3.2.6 Real-time solar wind data

Advanced Composition Explorer
s/c figure, launch date was 25 August 1997

MAG – fluxgate magnetometer
SWEPAM

data errors/gaps...

DSCOVR as replacement was launched on 11 Februar 2015. It is NOAA's SWPC real-time solar wind prime source since 27 July 2016.³

³<http://www.swpc.noaa.gov/products/real-time-solar-wind>

4 PaperMVVB

4.1 Literature

Schwenn1983 intro -> sw-averaging comment (beer and wine)

see Hellinger2013 p.1353

see astro70/CGAUSS/dropbox_presis/... (presi 1.07 Inside Helios-Origins and Evolution-Salem.ppt
-> Helios reloaded; radial functions for all parameters)

see Balogh1999 from p. 162 (Helios CIR results)

see Marsch1999... (model constraints)

model boundary condition: continuity of mass flux

On solar wind acceleration and SPP proposition: McComas2007

Motivational question: What is the evolution of the solar wind parameters/structures before arriving at Earth?

what is meant by the term evolution?

4.2 Seasonal solar wind variations

seasonal variation by month

quantify variation amplitudes

see [Figure 4.1](#)

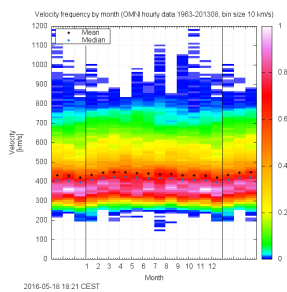


Figure 4.1 Diagram of the velocity frequency by month for the period 1963/01–2013/08. Mean and median values are shown as well.

see [Figure 4.2](#)

derived exponent values from simple trigonometric fit on monthly values:

$$c_N = -2.234$$

maybe figure?

expected influence from Earth's perihelion/aphelion (see Appendix...) distance vs observations
we expect for the proton density (scaling law $N(r) = 7.6 \text{ cm}^{-3} \cdot r^{-2}$):

$$N(0.983 \text{ au}) = 7.9 \text{ cm}^{-3}$$

$$N(1 \text{ au}) = 7.6 \text{ cm}^{-3}$$

$$N(1.017 \text{ au}) = 7.3 \text{ cm}^{-3}$$

we expect for the magnetic field strength (scaling law $\propto r^{-1.6}$):

$$B(0.983 \text{ au}) = 6.3 \text{ nT}$$

$$B(1 \text{ au}) = 6.1 \text{ nT}$$

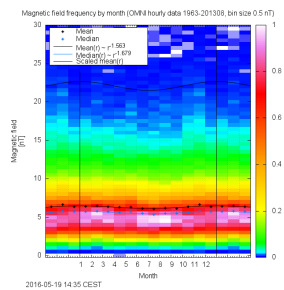


Figure 4.2 Diagram of magnetic field frequency by month for the period 1963/01–2013/08. Mean and median values are shown as well as the expected course from the solar distance variation (obtained from Helios data).

$$B(1.017 \text{ au}) = 5.9 \text{ nT}$$

4.3 Latitude dependency

refer to Ulysses figure...

Ulysses swoops polar plots...

see Schwenn1990's Fig. 3.14

see also Schwenn (1990) p. 127

see also Richardson et al. (1995)

latitude; see Figure 4.3

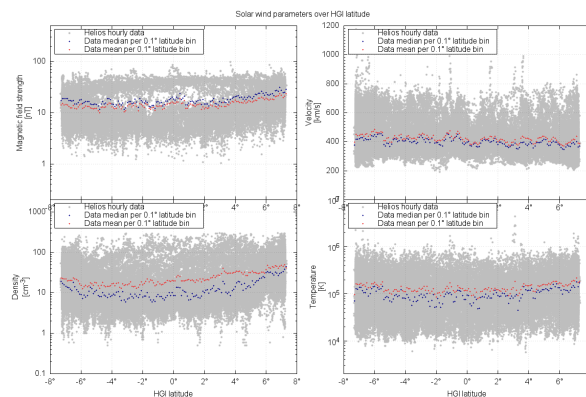


Figure 4.3 The four solar wind parameter's HGI latitude dependency. Their mean values per 0.1° bin are plotted as well. make figure same dimensions as projected figure in analysis part...

with the exponential dependencies to 1 au projected solar wind parameters; there are only small changes with latitude in the range -7.25° – 7.25°

have a look on distribution widths...

dependence from latitude in interval -7.25° – 7.25° in Helios data negligible?, see Figure 4.4. estimate error ranges...

plot Ulysses data into plot...

influence from latitude variation in data negligible? (see Ulysses figure in introduction). Helios probes within ecliptic => variation span equal to solar tilt: -7.25° to 7.25° ; solar tilt/obliquity to ecliptic: $i_\odot = 7.25^\circ$ (Sun fact sheet: <http://nssdc.gsfc.nasa.gov/planetary/factsheet/sunfact.html>)

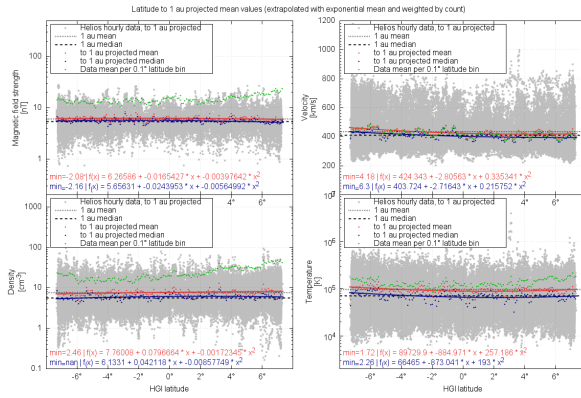


Figure 4.4 Plot of the to 1 au projected solar wind parameters over latitude. And their mean values, including weighted fit. add projected median...

big part of Helios data is from latitudes $> \pm 5^\circ$, see Figure XX (data count over latitude) and see Figure XX (Helios orbit polar plane in data section...)

4.4 Radial evolution of solar wind structures

Helios event lists HSSs, SLOWs, CIRs, CMEs...; event lists for all Helios data see Liu2004 for Helios ICME list and radial dependencies of B, n, T and v...

200 km/s slow solar wind at $10 R_\odot$ is in agreement with blob measurements from Wang2000

very slow sw (VSSW) gets accelerated; see Sanchez-Diaz2016:

structure extrapolations

radial diameter of MCs increase between 0.3 au and 4.3 au proportional to the distance as $r^{0.8}$ (Bothmer & Schwenn 1998)

MC central axial magnetic field strength radial density dependence $B = 18.1 r^{-1.64}$ Leitner et al. (2007)

MC average diameter $D = 0.23 r^{1.14}$ Leitner et al. (2007)

sw structure marked plot

4.5 Solar distance dependency—theory

B-field radial profile: $B \propto r^{-1.5}$?

Magnetic field magnitude model (Kivelson 1995):

$$Br(r) = B_0 / r^2$$

$$B\phi(r) = -B_0 \omega / (V_r * r) \text{ (shear effect from solar rotation omega)}$$

$$B\theta(r) = 0$$

$$B(r) = (Br^2 + B\phi^2 + B\theta^2)^{1/2}$$

see also [radial_fit_B_test_plot.png](#)

Parker references

velocity radial profile: $V \propto r^0$?

model based on LeBlanc1998 electron density with flux conservation: Zic2015(Temmer)

density radial profile: $N \propto r^{-2}$

simple view: for a spherical constant velocity mass outflow a one over distance squared law is expected, because of the mass flux conservation per solid angle for different distances. measurements up to the outer heliosphere confirm the $1/r^2$ dependency (1–38 au by Voyager 2, (Belcher et al. 1993) newer

paper?)

in an ideal neutral plasma the electron and proton number density have the same values (neutral plasma) (reference?)

ca. 10 % more electrons than protons (due to alphas) cite?

temperature radial profile: $T \propto r^{-1}$?

at larger distances heating outbalances the adiabatic temperature part (adiabatic cooling vs. pickup proton and stream-interaction heating; 1–68 au by Voyager 2; [Richardson & Smith \(2003\)](#))

solar wind ram pressure $p_{\text{ram}} = \rho V^2$

4.6 flux conservation

conserved quantities:

- momentum conservation... VBbookp112
- flux conservation...

With consideration of continuity the mass flux per solid angle has to be constant: $\dot{m} = \text{const}$

conserved quantities:

- mass flux: $\dot{m} = \rho v A$ (with mass density ρ , velocity v and [cross-sectional area A] or solid angle?...)
- particle fluxes (proton flux, electron flux, etc.)
- proton flux: $j_p = n_p v_p A$ (with proton density n_p and proton velocity v_p)

(with proton mass density $\rho = n_p m_p$ (with proton number density n_p and proton mass m_p)).

the individual radial dependencies for a spherical radial outflow are:

$$A(r) \propto r^2 \rightarrow A/r^2 = \text{const}$$

and assuming an exponential dependency,

$$n_p(r) = n_0 r^{c_n},$$

$$v(r) = v_0 r^{c_v}$$

$$j_p = \text{const} \quad (4.1)$$

$$n_p v_p A = \text{const} \quad (4.2)$$

$$n_0 r^{c_n} v_0 r^{c_v} r^2 = \text{const} \quad (4.3)$$

$$r^{c_n} r^{c_v} r^2 = \text{const} \quad (4.4)$$

$$\Rightarrow c_n + c_v + 2 = 0 \quad (4.5)$$

$$c_n + c_v = -2 \quad (4.6)$$

an increasing velocity should result in a steeper density...

validity of mass flux continuity: within the heliosphere mass to energy conversion and vice versa is negligible, but there can be flux from and to higher latitudes as the Helios data is localized to a small latitude range in the ecliptic plane.

estimate the error from that... (if error is too big => drop continuity condition)

larger errors should be located near CMEs and CIRs (nonradial flows from interactions)

there is a proton flux difference between slow and fast solar wind streams (see book Schwenn1990 p. 146)

estimate the possible size of error:

mean:

$$c_n = -2.010$$

$$c_v = 0.049$$

$$c_n + c_v = -1.961$$

difference to -2 is 0.039

4.7 sw parameters and precision

definition of 'the four solar wind parameters':

magnetic field strength, aka magnetic field, B , usually measured in nT, in the order of 0–35 nT at 1 au

proton bulk velocity, aka velocity, v , usually measured in km/s, in the order of 200–900 km/s at 1 au

proton number density, aka density, n , usually measured in cm⁻³, in the order of 1–60 at 1 au

proton temperature, aka temperature, T , usually measured in K, in the order of 10 000–1 000 000 K at 1 au

sentence about ordering of the parameters...

hourly OMNI data

measurement precision:

B : 0.01 nT

v : 1 km/s

n : 0.1 cm⁻³

T : 1 K ? (smallest found: 7 K)

error discussion:

OMNI hourly data mean:

B : bin size 0.5 nT, median 5.6, mean 6.30056(18)

v : bin size 10 km/s, median 414, mean 437.6700(18)

n : bin size 1 cm⁻³, median 5.3, mean 6.831410(18)

T : bin size 10 000 K, median 80 751, mean 112 219.0(19) (with 1000 K as precision)

empirical data; Helios; hourly

why hourly and not higher resolution data?

measurement precision:

B : 0.01 nT

v : 0.1 km/s

n : 0.1 cm⁻³

T : 100–1000 K (3 digits)

r : 0.01 au

error discussion:

Helios hourly data mean:

B : min 337, precision: 0.000545; 18.3x better

v : min 497, precision: 0.00449; 22.2x

n : min 497, precision: 0.00449; 22.2x

T : min 497, precision: 4.49–44.49 22.2x

=> so we use 1/10 the measurement precision for the mean.

median precision same as data precision

Helios histogram bin size for mean of frequency distribution (at specific solar distance)

B : bin size 0.5 nT, min 337, mean precision: 0.000545

v : bin size 1 cm⁻³, min 497, mean precision: 0.00449

n : bin size 10 km/s, min 497, mean precision: 0.00449

T : bin size 10 000 K, min 497, mean precision: 4.49–44.49

4.8 other

McGregor2011 analyzed the empirical magnetic topology–velocity relationship, using Helios perihelion data with the Wang-Sheeley-Arge (WSA) coronal model, and found indications, that the fast and slow solar wind are generated from distinct sources. (not only superradial expansion)

Larger individual graphs can be found in the appendix...

state this at the first occurrence... (from GUM guide)
 $mS = 100,021\ 47(35)\ g$, where the number in parentheses is the numerical value of (the combined standard uncertainty) uc referred to the corresponding last digits of the quoted result.

For more on lognormal distributions see appendix [section B.2](#)

we get the ultimate monster equation:

$$W_{II}(x, \tilde{a}_1, \tilde{b}_1, \bar{a}_1, \bar{b}_1, \tilde{a}_2, \tilde{b}_2, \bar{a}_2, \bar{b}_2) = \quad (4.7)$$

$$\frac{c}{2\sqrt{\pi \ln\left(\frac{\bar{a}_1 r^{\tilde{b}_1}}{\tilde{a}_1 r^{\tilde{b}_1}}\right)} x} \exp\left(-\frac{\ln^2\left(\frac{x}{\tilde{a}_1 r^{\tilde{b}_1}}\right)}{4 \ln\left(\frac{\bar{a}_1 r^{\tilde{b}_1}}{\tilde{a}_1 r^{\tilde{b}_1}}\right)}\right) + \frac{(1-c)}{2\sqrt{\pi \ln\left(\frac{\bar{a}_2 r^{\tilde{b}_2}}{\tilde{a}_2 r^{\tilde{b}_2}}\right)} x} \exp\left(-\frac{\ln^2\left(\frac{x}{\tilde{a}_2 r^{\tilde{b}_2}}\right)}{4 \ln\left(\frac{\bar{a}_2 r^{\tilde{b}_2}}{\tilde{a}_2 r^{\tilde{b}_2}}\right)}\right) \quad (4.8)$$

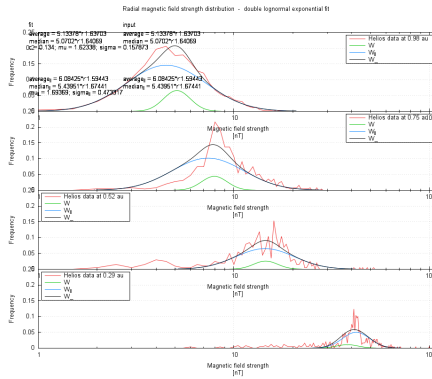


Figure 4.5 Plot of the magnetic field strength's frequency distribution at different solar distances (0.29, 0.52, 0.75 and 0.98 au). The Helios data, the composed fit model and both its components are plotted. 0.23 au steps, lw 2, stepfunction

=> what kind of distribution has the B-field near the Sun?

The extrapolation distance is only about one third of the model range, but as the parameters follow exponential change, one has to look at the logarithmic distance which is indeed one and a half times the model range.

argument with gravitational deceleration; near-Sun extrapolation should be biased, because in the near-Sun region gravitation becomes significant (see [Figure 4.6](#))

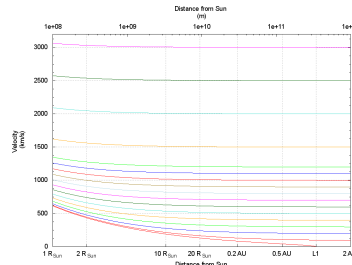


Figure 4.6 velocity over solar distance; gravitational deceleration. place instead figure of grav. force over solar distance...

comparison...

...with Vourlidas estimates at $10 R_\odot$

...with Wang2000 slow blobs

5 Helios radial line-up passings

have a look into Schwenn1984...

To derive the radial dependence of the solar wind parameters directly, we look at the passings when both Helios spacecraft were radially lined up. In these cases they flew through the same solar wind at different solar distances.

(This eliminates the bias of averaging over slow and fast wind streams, like the described model does.) see also [Schwenn \(1990\)](#) p. 156 + p. 122...

we compare these independently derived radial fit functions to those obtained from the averaging over all solar wind types...

There were eight passings when both Helios spacecraft were radially lined-up (see [Figure 5.1](#)). These points in time, when both probes had no separation in heliographic longitude, are derived from

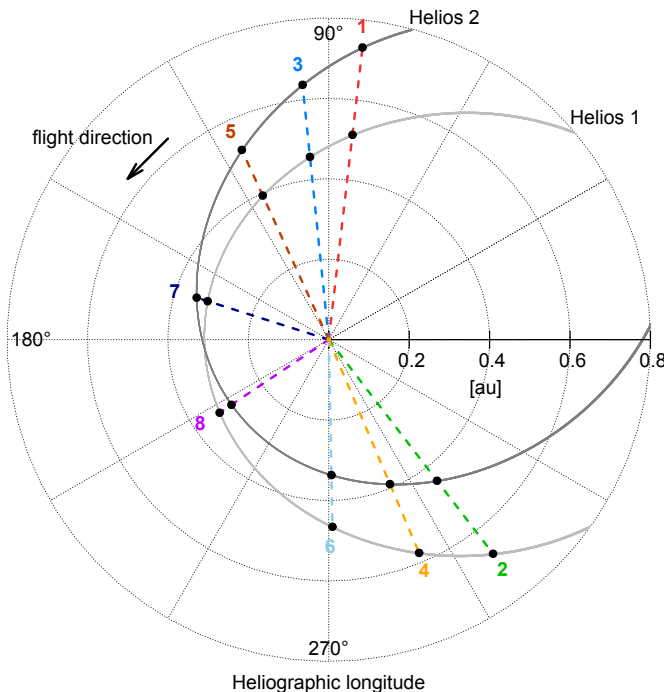


Figure 5.1 Schema of the eight spacecraft line-up positions of both Helios probes on their respective orbits. make B&W... combine with fig 5.15? calibrate text size

Helios 1 and Helios 2 daily trajectory data (for the data source see Section XX). The data is linear interpolated to get an hourly resolution. The resulting points in time together with solar distances are listed in [Table 5.1](#).

The last two passings were merely one week apart and the Helios probes flew almost without radial separation because Helios 2 overtook Helios 1 during its perihelion. As we want to analyze the same solar wind at different solar distances, we exclude the passings 7 and 8 from further analyses.

The passing longitude is not the same as the longitude where the solar wind is detected by both spacecraft consecutively. A passing occurs shortly before the points in time when both spacecraft observe the same solar wind. For the outer probe this point in time is shifted by the solar wind's travel time. The travel time depends on the solar wind's velocity and its distance traveled.

5. Helios radial line-up passings

Table 5.1 Times when both Helios probes had no separation in heliographic longitude. Their solar distances (inner spacecraft r_1 , outer spacecraft r_2) were in the range 0.291–0.731 au and the maximal inter-probe radial distance dr was 0.229 au. errors in au...

Passing	Date	Time	Inner s/c	r_1 [au]	r_2 [au]	dr [au]
1	1976-03-09	00:00	Helios 1	0.513	0.731	0.219
2	1976-05-02	14:00	Helios 2	0.442	0.671	0.229
3	1976-09-19	10:00	Helios 1	0.457	0.637	0.180
4	1976-10-31	11:00	Helios 2	0.390	0.576	0.186
5	1977-04-02	12:00	Helios 1	0.394	0.519	0.125
6	1977-04-30	23:00	Helios 2	0.337	0.465	0.128
7	1977-10-18	06:00	Helios 1	0.316	0.345	0.029
8	1977-10-25	19:00	Helios 2	0.291	0.327	0.035

Based on the obtained spacecraft line-up time t_0 one can calculate the offset times t_1 and t_2 when the inner and outer spacecraft pass by the same solar wind (see Figure 5.2). At the solar wind line-up longitude the condition

$$t_2 = t_1 + t_{sw} \quad (5.1)$$

holds. As the offset times depend on the solar wind travel time between the probes, we need knowledge of the solar wind velocity v for their calculation: $t_{sw} = dr/v$, with the mean radial separation distance dr between the probes.

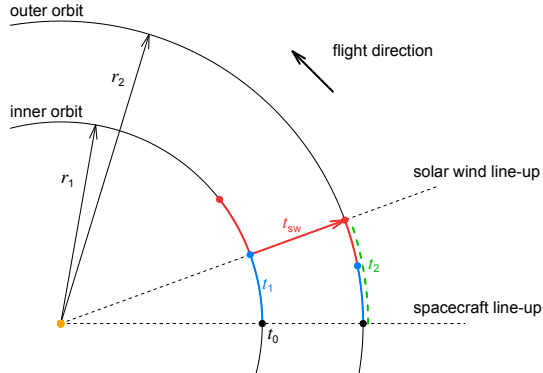


Figure 5.2 Illustration of the solar wind line-up longitude situation with the spacecraft line-up time t_0 , the offset times t_1 , t_2 (at which the spacecraft measure the same solar wind) and the solar wind travel time t_{sw} . combine with fig 5.14?

For the calculation of t_1 we recall the third Kepler law

$$\frac{T_1^2}{T_2^2} = \frac{a_1^3}{a_2^3} \quad (5.2)$$

with the orbital periods T_1 , T_2 and the semi-major axes a_1 , a_2 . The assumption of circular orbits (why? what error size?) leads to

$$\begin{aligned} \frac{t_1^2}{(t_1 + t_{sw})^2} &= \frac{r_1^3}{r_2^3} \\ \Leftrightarrow \quad t_1 &= t_{sw} \left(\left(\frac{r_1}{r_2} \right)^{\frac{3}{2}} - 1 \right)^{-1} \end{aligned} \quad (5.3)$$

and finally the offset time t_1 only depends on the variable solar wind travel time t_{sw} .

Due to uncertainties in the travel time t_{sw} (the solar wind speed v is obviously not a constant) the exact calculation of t_1 is imprecise. To get a reliable result we perform two iterations calculating the offset time from the average velocity \bar{v} of the surrounding 2-day period. We use the velocity \bar{v}_0 around t_0 to calculate the offset time t'_1 as a first estimate. As the velocity \bar{v}'_1 at t'_1 is certainly different, we use this velocity to refine the value and obtain t_1 . Hence deriving the velocity \bar{v}_1 enables us to calculate the solar wind travel time t_{sw} .

The average velocities are obtained from the hourly merged (mag?) and (plasma?) Helios data set (see Section XX). The resulting offset times and velocities of both iterations together with the travel times are listed in [Table 5.2](#).

Table 5.2 The two iterations of the derived offset times and average velocities. The resulting solar wind travel times have durations of 11–28 hours. errors...

Passing	Inner s/c	v_0 [km/s]	t'_1 [h]	v'_1 [km/s]	t_1 [h]	v_1 [km/s]	t_{sw} [h]
1	Helios 1	659.3	19.6	656.9	19.7	656.9	13.9
2	Helios 2	436.4	25.1	370.9	29.5	356.7	26.7
3	Helios 1	482.6	24.0	444.0	26.1	413.8	18.1
4	Helios 2	302.3	32.2	279.9	34.8	278.3	27.8
5	Helios 1	507.3	20.0	474.8	21.4	473.5	11.0
6	Helios 2	321.2	26.6	392.6	21.7	367.8	14.5

For the solar wind line-up longitude condition (5.1) holds. For all other positions the solar wind measured by the inner spacecraft will not arrive the outer orbit position at the same time as the outer spacecraft does (see [Figure 5.3](#)).

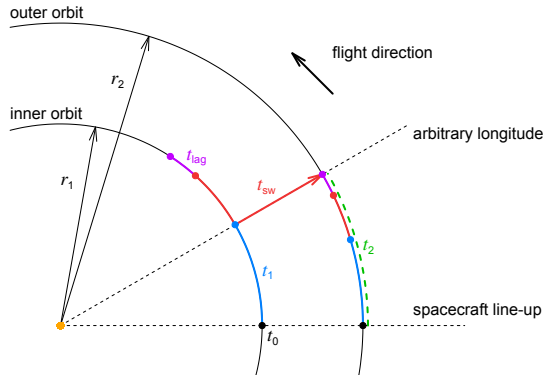


Figure 5.3 Illustration like [Figure 5.2](#) but for arbitrary longitude situations a lag time t_{lag} comes into play. merge with fig 5.14?

Either the spacecraft (negative lag time) or the solar wind (positive lag time) already have passed this position:

$$t_2 = t_1 + t_{\text{sw}} + t_{\text{lag}}. \quad (5.4)$$

This lag time t_{lag} is the time difference at which the solar wind is probed by both spacecraft. At the spacecraft line-up longitude ($t_1 = t_2 = 0$) the lag time equals the solar wind travel time and at the solar wind line-up longitude the lag time is zero.

We choose to look at time periods (instead of points in time) around the offset times to derive average solar wind parameters. This helps reducing the influence of solar wind fluctuations.

We define the period duration boundaries as when the lag time t_{lag} is in the range ± 24 h. For the outer spacecraft these periods are almost twice as long as for the inner spacecraft. The calculated period start and end hours (relative to t_0) for both spacecraft are listed in [Table 5.3](#) together with the data coverage of these periods.

5. Helios radial line-up passings

Table 5.3 Derived period start and end hours for both spacecraft in relation to the longitude line-up time t_0 . The corresponding combined data coverage within that period of the magnetic field, velocity, density and temperature is listed as well. instead duration! errors...

Period	s/c	Inner spacecraft			Outer spacecraft		
		Start [h]	End [h]	Coverage [%]	Start [h]	End [h]	Coverage [%]
1	Helios 1	-14.4	53.8	73	-24.6	91.6	99
2	Helios 2	3.1	58.3	89	5.8	109.0	88
3	Helios 1	-9.2	65.1	16	-15.1	107.2	10
4	Helios 2	4.8	65.2	59	8.5	117.0	87
5	Helios 1	-25.5	68.3	89	-38.5	103.3	88
6	Helios 2	-15.3	61.7	93	-24.8	100.1	92

For period 3 the combined data coverage of the four solar wind parameters is only 16 % (Helios 1) and 10 % (Helios 2) respectively. We consider this as insufficient for the continuing analysis and therefore also omit period 3.

The five remaining periods are marked in [Figure 5.4](#).

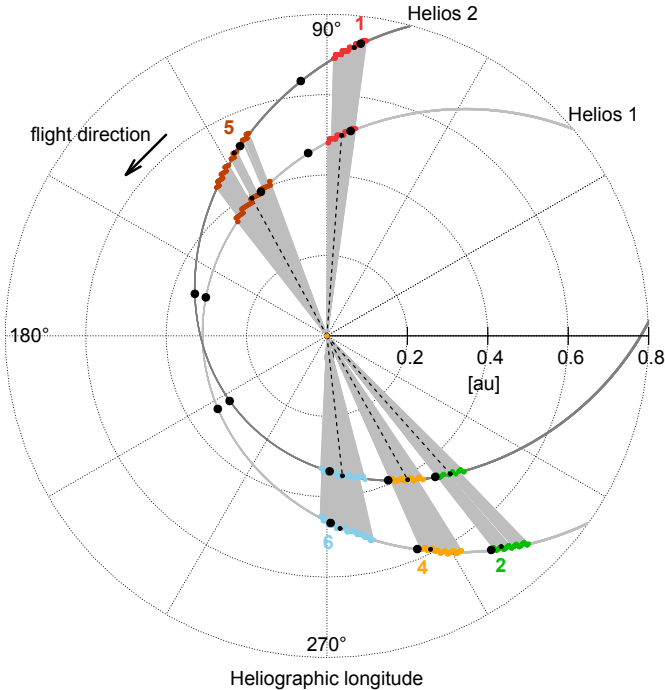


Figure 5.4 Scheme of the line-up periods of both Helios spacecraft on their respective orbits. The corresponding orbit sections which we consider in our analysis are marked in color. These sections span the positions where both spacecraft observed the same solar wind with a maximal lag time of ± 24 hours. bw figure?? dotted lines?

The average values of the four parameters magnetic field B , velocity v , density n and temperature T are listed in [Table 5.4](#).

If we compare both, the inner solar wind sections together with their outer counterparts, they indeed appear to have a similar shape apart from the time shift (see [Figure 5.5](#)) (name definite features...). This confirms that they indeed are parts of the same solar wind structures.
maybe figures of all into Appendix?...

the comparison to the sw model's mean value at the individual distances lets us classify the solar wind types...

Period 1 HSS

Table 5.4 Average values of the four solar wind parameters magnetic field, velocity, density and temperature for the individual periods and spacecraft. errors...

Period	s/c	Inner spacecraft				Outer spacecraft			
		B [nT]	v [km/s]	n [cm ⁻³]	T [K]	B [nT]	v [km/s]	n [cm ⁻³]	T [K]
1	Helios 1	17.04	646.4	12.0	367 300	8.93	602.8	6.7	244 000
2	Helios 2	15.77	356.4	38.8	122 400	12.05	390.2	17.7	117 200
4	Helios 2	15.18	281.3	108.0	46 000	10.64	298.6	46.1	30 400
5	Helios 1	28.80	521.3	45.9	337 800	18.73	530.3	24.4	282 000
6	Helios 2	29.57	402.4	82.5	271 900	14.71	432.6	35.7	199 100

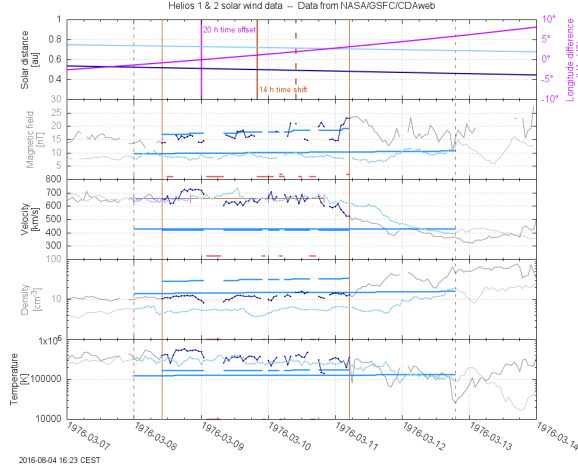


Figure 5.5 Measured solar wind parameters B , v , n , and T of both spacecraft in the period 1. Also plotted is the spacecraft's separation in heliographic longitude. offset time, time shift; expected value from the radial sw model... remove date... remove solar distance... adjust text size...

Period 2 medium-LSS

Period 4 LSS

Period 5 medium-HSS

Period 6 LSS-HSS

We obtained the mean parameter values for the inner and outer solar wind sections. As with the overall radial dependency before, these two points are fitted to the exponential regression fit function $X(r) = X_0 r^{cx}$ (see Section XX. The resulting fit coefficients for each period are listed in **Table 5.5**. why is it better to fit the period's mean values than the whole period?... we fit the periods' mean value rather than the whole periods, because...

Table 5.5 Radial fit functions $B(r)$, $v(r)$, $n(r)$ and $T(r)$ for each period. or only the variables into table? error sizes...

Period	$B(r) = B_0 r^{cb}$ [nT]	$v(r) = v_0 r^{cv}$ [km/s]	$n(r) = n_0 r^{cn}$ [cm ⁻³]	$T(r) = T_0 r^{ct}$ [K]
1	$4.88 r^{-1.815}$	$564.7 r^{-0.196}$	$3.9 r^{-1.647}$	$166\,500 r^{-1.148}$
2	$9.50 r^{-0.654}$	$442.6 r^{0.220}$	$8.9 r^{-1.902}$	$112\,800 r^{-0.106}$
4	$6.79 r^{-0.900}$	$322.0 r^{0.151}$	$15.7 r^{-2.155}$	$18\,000 r^{-1.047}$
5	$5.99 r^{-1.649}$	$554.8 r^{0.065}$	$4.6 r^{-2.423}$	$174\,700 r^{-0.692}$
6	$3.22 r^{-2.108}$	$506.5 r^{0.219}$	$5.7 r^{-2.533}$	$101\,000 r^{-0.941}$

weighted by duration mean functions

mean of sw model (update)	$6.078 r^{-1.563}$	$435.5 r^{0.04955}$	$7.613 r^{-2.032}$	$97\,050 r^{-0.8002}$
---------------------------	--------------------	---------------------	--------------------	-----------------------

The fit curves show noticeable deviations from the model's mean fit (see [Figure 5.6](#)). maybe 4-panel

5. Helios radial line-up passings

figure?; maybe figures of all into Appendix?

The observed deviations are as expected from these types of solar wind. ...are they? analyze each in

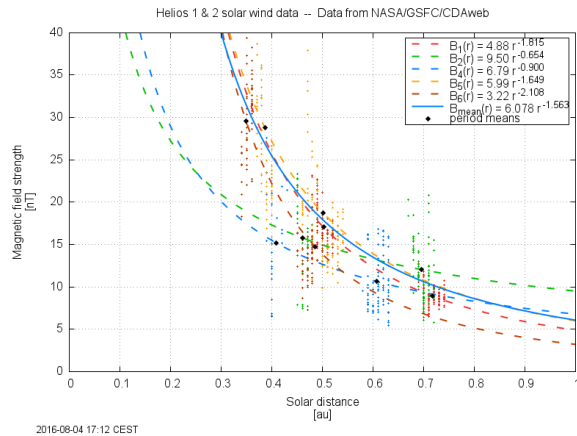


Figure 5.6 Fit curves of the radial magnetic field. The fits are based on the mean values (meanr,meanB; black points) of the line-up periods. build pdf figure... remove date... adjust text size... 4-figure?

detail...

argue from sw type; slow, medium and fast type; check their position relative to the mean curve...

results:

features of calculated line-up periods match.

their derived fit functions scatter within (acceptable?) margin around model's radial mean, backing its applicability.

6 chapter2

Alle Presis ausschlachten!
Alle Projektberichte ausschlachten!
Kp8–Liste irgendwo einweben...
paper draft 2014 ausschlachten... Check!

-> example events CIR/HSS and CME

literature:

SWS: Rules of the Road: Please contact Ian Richardson about your use of this data.
V-Kp correlation similar to [Elliott et al. \(2013\)](#); different data resolution and averaging method (3-hour maximum of 1 min data)
linear velocity replacement of ACE realtime data with Kp, Machol2013

6.1 Solar wind interaction processes with the magnetosphere

there are several underlying physical mechanisms, whose contribution is not yet quantified'?'
physical mechanisms:

- reconnection
- compression
- turbulence
- induction?

three ways for solar wind momentum and energy transfer into magnetosphere:
- sw entering sphere
- waves/eddies
- reconnection

6.2 Solar wind–magnetosphere coupling functions

coupling mechanisms and therefrom derived functions
VBzgsm - E-field...

Studies finding best coupling function, Newell, etc.

[Newell et al. \(2007\)](#): universal sw-magnetosphere coupling function (opening flux rate)
[Newell et al. \(2008\)](#): coupling function merging and viscous term
merging and viscous terms (reconnection and turbulence)
merging term: rate magnetic flux is opened at the magnetopause ($d\Phi_{MP}/dt$)
viscous term: reconnection due to Kelvin-Helmholtz instabilities at the boundary ($n^{1/2}v^2$)
equation for the least variance linear prediction of Kp: $Kp = 0.05 + 2.244 \times 10^{-4} d\Phi_{MP}/dt + 2.844 \times 10^{-6} n^{1/2} v^2$
combination of both terms works best ($r = 0.866$)

see also [subsection 2.6.4](#)

6.3 Parameter selection

In our analyses we use the planetary geomagnetic disturbance indicator Kp (see Section XX...), because it is designed to measure solar particle radiation by its magnetic effects (cite? Bartels...?).

and has close relation to aurorae, NOAA scale

correlation coefficients in [Table 6.1](#).

Table 6.1 Pearson correlation coefficients of Kp with solar wind parameters... (use Spearman instead?)

Parameter	OMNI 1min	
	19850101-20150101	3h 1min max
N	0.199792	
V	0.598351	
T	0.510607	
B	0.595860	
Bzgsm	-0.666050 ^a	
V*B	0.682383	
V*Bzgsm	-0.715101 ^a	
N*T		

^aHere it is min instead of max.

6.4 Data selection

choosing data time range

the Kp time series started in XXXX, when there were no spacecraft to measure in situ solar wind -> time range defined by available solar wind data

OMNI data set -> longest continuous solar wind data set

6.5 Solar cycle influence

solar cycle dependence

- parameter time plots
- parameter vs SSN matrix-plots
- cc time plots
- cc vs SSN plots

6.6 CME correlations

same analysis for CMEs

- parameter time plots
- parameter vs SSN matrix-plots
- cc time plots
- cc vs SSN plots

6.7 Solar wind structure analyses

How strong do different structure types influence the terrestrial magnetosphere?

What kind of solar wind structures create the individual regions in this distribution?

What is their individual contribution to the Kp ranges (e.g. high Kp: CMEs 70% and CIRs 30%)?

ACE solar wind time series and event list

sw-timeseries ACE OPTIMAP “Zeitreihe”-events

method: automatic list creation by event detection via parameter thresholds...

sample CME analyses (MVA, -> K_p)

(How can the impact field strength of CMEs be forecasted (V->B correlation for CMEs)?)

6.8 Forecast

Internal solar wind correlations:

B-V correlation

ACE MAGSWE 64 s data -> yearly overlay plot

applications:

rssfeeds, rtsw plots

CME K_p impact as part of DDC

- K_p nowcast with L1 solar wind measurements (L1 alerts, disseminated as RSS feeds; integrated in smartphone app and space weather display)
- Forecast of the possible CME impact on the Earth's magnetosphere (K_p index) from the predicted CME arrival velocity (integrated in UGOE CME forecast chain (aka DDC))

seasonal correction: $\Delta K_p(\text{month})$

$$K_{p\text{impact}} = K_{p\text{CME}} \pm \Delta K_p(\text{month})$$

7 Discussion/conclusions/results

results
discussion
conclusions
summary
outlook

Prediction:
Long-term solar wind parameter predictions from SSN
Link from near-Sun solar wind measurements to Kp impact
Link from near-Sun structure (CMEs, CIRs) measurements to Kp impact

8 Summary and outlook

Outlook

DSCOVR data (advantages over ACE? gain?)
anticipated Solar Probe Plus data (near-Sun data)

other possible space weather missions: sub-L1 (earlier in situ CME magnitude warning) and L5 (early CME velocity and arrival warning)

I built an empirical solar wind model for the ecliptical inner heliosphere which accounts for variations in time (season and solar cycle) and space (solar distance).

Using the SSN prediction the model allows the forecast and extrapolation of the solar wind, which will occur during the SPP mission's first near-Sun perihelia in mid-2018.

A Physics

A.1 Electromagnetism

Electromagnetism is one of the four fundamental forces at the common level of energy. In all situations examined in this thesis (sw plasma, magnetosphere) it is by far the strongest force and the others can be neglected.

The Lorentz force: $\mathbf{F} = q(\mathbf{E} + \mathbf{v} \times \mathbf{B})$

The Maxwell equations in differential notation:

$$\operatorname{div} \mathbf{B} = 0 \quad (\text{A.1})$$

$$\operatorname{div} \mathbf{D} = \rho \quad (\text{A.2})$$

$$\operatorname{rot} \mathbf{H} = \mathbf{j} + \dot{\mathbf{D}} \quad (\text{A.3})$$

$$\operatorname{rot} \mathbf{E} = -\dot{\mathbf{B}} \quad (\text{A.4})$$

With the magnetic flux density \mathbf{B} (aka magnetic field), the electric displacement field \mathbf{D} , the charge density ρ , the magnetic field \mathbf{H} , the electric field \mathbf{E} and the current density \mathbf{j} .

A.2 Solar wind pressures

The magnetic energy density w_{mag} is also the magnetic pressure p_{mag}

$$w_{\text{mag}} = p_{\text{mag}} \quad (\text{A.5})$$

$$= \frac{B^2}{2\mu_0}. \quad (\text{A.6})$$

dynamic pressure $p_{\text{dyn}} = \rho v^2$
 thermal pressure $p_{\text{therm}} = nk_B T$
 magnetic pressure $p_{\text{mag}} = B^2/(2\mu_0)$ (see above...)
 ram pressure??

A.3 Plasma beta

In MHD the magnetic energy density behaves like an additional pressure that adds to the gas pressure of a plasma (Wikipedia; find alternative source...).

The ratio of the thermal pressure $p = nk_B T$ to the magnetic pressure $p_{\text{mag}} = \frac{B^2}{2\mu_0}$ is called plasma beta

$$\beta = \frac{p}{p_{\text{mag}}} \quad (\text{A.7})$$

$$= \frac{2\mu_0 n k_B T}{B^2} \quad (\text{A.8})$$

with the number density n .

$\beta \ll 1$: “cold” plasma; magnetic field contains plasma (magnetic clouds)

$\beta \geq 1$: “warm” plasma; plasma keeps magnetic field

plasma beta see ([Kivelson & Russell 1995](#), p. 50)

typical *beta*-values for solar wind are in the range X–Y.

A.4 Alfvén waves

named after Hannes Alfvén...

There exists an incompressible wave mode which is a result of bending magnetic field lines called shear Alfvén wave.

In an ideal incompressible MHD plasma (viscosity $\mu = 0$ and electrical conductivity $\sigma = \infty$) the kinetic and magnetic energy density are of equal value:

$$w_{\text{kin}} = w_{\text{mag}} \quad (\text{A.9})$$

$$\frac{\rho v^2}{2} = \frac{B^2}{2\mu_0}$$

with the permeability constant

$$\mu_0 = 4\pi \cdot 10^{-7} \text{ N A}^{-2}$$

and the total mass density ρ of the charged plasma particles.

So waves propagate with the so-called Alfvén velocity

$$v_A = \frac{|B|}{\sqrt{\mu_0 \rho}}. \quad (\text{A.10})$$

Their phase velocity is

$$v_{\text{ph}} = v_A \cos(\theta) \quad (\text{A.11})$$

with θ the angle between wave propagation direction (k) and magnetic field line (B). \Rightarrow Alfvén waves travel along magnetic field lines. Alfvén waves are characterized by periodic disturbances in the magnetic field perpendicular to its direction, in the electric field, in the plasma velocity and in the current density. They do not affect the plasma density, plasma pressure and magnetic field magnitude.

Additionally, there exist two types of compressional waves within MHD plasmas, the fast-mode wave and the slow-mode wave. The phase speeds of the three MHD waves meet $v_{\text{fast}} \geq v_A \geq v_{\text{slow}}$.

Alfvén waves are dominant in regions that are open to the heliosphere.

Alfvén waves see (Kivelson & Russell 1995, pp. 51ff.)

Within average solar wind at 1 au their typical frequency is 1–4 per hour (cite?) ($v_A = 53 \text{ km/s}$ for $B = 5.6 \text{ nT}$ and $\rho = 5.3 \text{ cm}^{-3}$).

critical surfaces, solar wind acceleration...

A.5 Solar surface differential rotation

the solar rotation was first discovered from sunspots in 18XX?

Bartels (1934) set the synodic solar rotation period to 27 days for the definition of his solar rotation number. The Bartels' Rotation Number counts the solar rotations starting with 8 February 1832. Carrington solar rotation period of 27.2753 days (Where Carrington Rotation Number is based upon, starting with November 9, 1853; Wikipedia...)

Solar surface rotation period at 16° latitude:

sidereal: 25.38 d (of 609.12 h Sun Fact Sheet...), synodic: 27.2753 d (derived)

rotation axis tilt (see next section)

The Sun's inner thermal convective circulation results in a differential rotation caused by transport of angular momentum away from the rotation axis.

The Sun's sidereal differential angular velocity best-fitting function with values as stated in (Sun Fact Sheet...)¹ is

$$\omega_{\odot} = A + B \sin^2(b) + C \sin^4(b) \quad (\text{A.12})$$

¹NASA's Sun Fact Sheet (<http://nssdc.gsfc.nasa.gov/planetary/factsheet/sunfact.html>, accessed 2016-08-19).

with the latitude b , the equatorial angular velocity $A = 14.37^\circ/\text{d}$, the coefficients $B = -2.33^\circ/\text{d}$ and $C = -1.56^\circ/\text{d}$ (see Figure A.1).

see Figure A.1

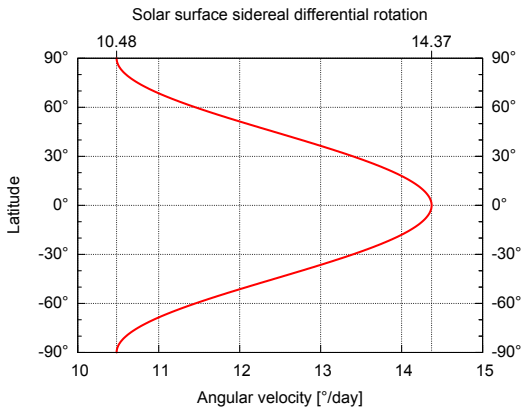


Figure A.1 Diagram of the sidereal solar surface differential rotation. It shows the angular velocity for different latitudes. remove sides...

Thus, the solar equatorial rotation period (sidereal) is

$$\begin{aligned} T_{\odot}^{\text{eq}} &= 360^\circ/A \\ &= 25.05 \text{ d} \end{aligned} \quad (\text{A.13})$$

and the synodic period is

$$\begin{aligned} T_{\odot}^{\text{eq,syn}} &= 1/(1/T_{\odot}^{\text{eq}} - 1/T_{\text{Earth}}) \\ &= 26.90 \text{ d} \end{aligned} \quad (\text{A.14})$$

with the Earth's orbital rotation period $T_{\text{Earth}} = 365.25 \text{ d}$ (1/100 Julian century).

Solar surface rotation period at equator
sidereal: 25.05 d (Sun Fact Sheet...), synodic: 26.90 d (derived)
Solar surface rotation period at poles:
sidereal: 34.35 d (diff. rot. formula), synodic: 37.92 d (derived)
are listed in Table A.1.

Table A.1 Solar surface rotation periods for equator, $\pm 16^\circ$ latitude and poles (sidereal and synodic).

	Equator [d]	$\pm 16^\circ$ latitude [d]	Poles [d]
Sidereal	25.05	25.38	34.35
Synodic	26.90	27.2753 ^a	37.92

^aCarrington solar rotation period

The meridional circulation is the proposed equatorial updrift and polar downdrift - a result of Reynolds stress and convective transport (cite?).

A.6 Earth orbit geometry

orbit defines ecliptic

Earth orbit parameters (cite?):
semimajor axis: $a = 1.000001018 \text{ au}$
eccentricity: $e = 0.0167086 \text{ au}$
distance at perihelion: (formula cite?, accuracy?)

$$\begin{aligned} r_p &= a(1 - e) \\ &= 0.98329 \text{ au} \end{aligned} \tag{A.15}$$

distance at aphelion:

$$\begin{aligned} r_p &= a(1 + e) \\ &= 1.0167 \text{ au} \end{aligned} \tag{A.16}$$

for calculation of heliospheric distance see HORIZONS Web-Interface at <http://ssd.jpl.nasa.gov/horizons.cgi>
perihelion/aphelion times...

A.6.1 Solar distance

A.6.2 Solar rotation axis tilt

The inclination of the solar equator to the ecliptic (tilt/obliquity) is $i_{\odot} = 7.25^\circ$ ([U.S. Nautical Almanac Office 2015](#)).

Viewed from Earth the projected solar rotation axis tilt angle varies as the Earth is moving on its orbit.

At the time XX the angle is zero.

The projected tilt angle to Earth over the year is

Hapgood (1992):

$$\omega = 73.67 + 0.013958 * (\text{today} - 1850.0) \tag{A.17}$$

solar tilt over the year, see [Figure A.2](#)

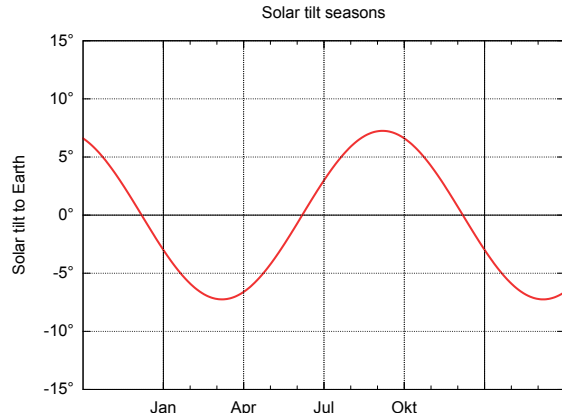


Figure A.2 Projected solar tilt angle over the year as viewed from Earth. remove sides...

A.6.3 Earth tilt

A.7 Coordinate systems

Coordinate systems used in this thesis:

GSE - Geocentric Solar Ecliptic

GSM - Geocentric Solar Magnetospheric

HGI - Heliographic Inertial

refer to [Hapgood \(1992\)](#) for GSE and GSM

figures for GSE and GSM

A.7.1 Geocentric Solar Ecliptic

The Geocentric Solar Ecliptic (GSE) coordinates are
GSE - Geocentric Solar Ecliptic
X = Earth-Sun Line
Z = Ecliptic North Pole
GSE coordinates are used in ACE solar wind data, etc.

A.7.2 Geocentric Solar Magnetospheric

GSM - Geocentric Solar Magnetospheric
X = Earth-Sun Line
Z = Projection of dipole axis on GSE YZ plane

GSM is defined with a time dependent dipole axis.
the dipole axis orientation changes over time; at 1995 the northern pole was at $l = 288.59^\circ$ and
 $b = 79.30^\circ$; more recent year (2015)?... cite?

A.7.3 Heliographic Inertial

HGI - Heliographic Inertial coordinates

B Math

B.1 Correlations

auto correlation

cross correlation

Pearson linear correlation

Spearman rank correlation

Correlation in Linear Regression: <http://www.stat.yale.edu/Courses/1997-98/101/correl.htm>

B.2 Lognormal distribution

This is a small summary about the lognormal probability distribution (Bronstein et al. 2000, p. 780). The lognormal distribution is the distribution of a random variable X if the logarithm of X conforms to a normal distribution. Its shape is highly asymmetric, however in a semi-log plot the Gaussian bell curve is recognizable (see the second panel of Figure B.1). Its probability density function is

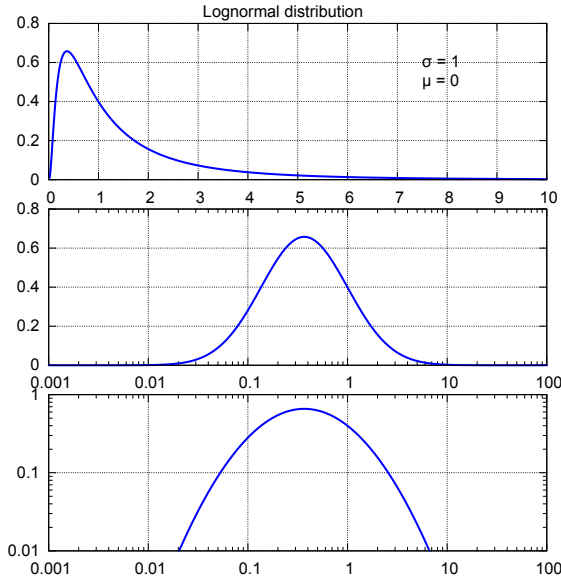


Figure B.1 The lognormal probability density function ($\sigma = 1, \mu = 0$) plotted in a linear, semi-log and log-log way. remove borders...

$$f(x) = \frac{1}{\sigma\sqrt{2\pi}x} e^{-\frac{(\ln x - \mu)^2}{2\sigma^2}} \quad (\text{B.1})$$

with the location (μ) and the shape parameter (σ). Changes in μ affect both the horizontal and vertical scaling of the function, whereas σ has an influence on its shape (see Figure B.2).

Because it is a probability distribution, its area is normalized

$$\int_0^\infty f(x)dx = 1. \quad (\text{B.2})$$

For a lognormally distributed random variable the geometric moments mean, standard deviation

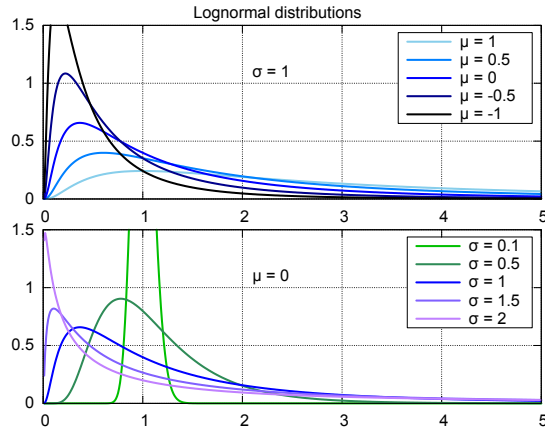


Figure B.2 Five lognormal distributions plotted with fixed σ (top) and fixed μ (bottom). remove borders...

and variance are:

$$\begin{aligned}\mu_g &= e^\mu, \\ \sigma_g &= e^\sigma, \\ var_g &= e^{\sigma^2} \quad (!).\end{aligned}$$

Its arithmetic moments are:

$$\begin{aligned}\mu_a &= e^{\mu + \frac{\sigma^2}{2}}, \\ \sigma_a &= e^{\mu + \frac{\sigma^2}{2}} \left(e^{\sigma^2} - 1 \right), \\ var_a &= \sigma_a^2.\end{aligned}$$

Other useful characteristics are the median and the mode

$$\begin{aligned}x_{\text{median}} &= e^\mu, \\ x_{\text{mode}} &= e^{\mu - \sigma^2}.\end{aligned}$$

Note that for the lognormal distribution its median is equal to its geometric mean.

Applications of lognormal distributions...

Most natural quantities which can only be positive are lognormally distributed. e.g. animal body sizes?, animal life expectancies, financial stock prices...; income distributions.

B.3 Goodness of fit

SSR – sum of squared residuals

$$SSR = \sum_i (y_i - f_i)^2 \tag{B.3}$$

data values y_i , fit function values f_i

SSR_{red} – reduced SSR, divided by number of degrees of freedom ν

$$SSR_{\text{red}} = \frac{SSR}{\nu} \tag{B.4}$$

TSS – total sum of squares (in relation to the data mean)

$$TSS = \sum_i (y_i - \bar{y})^2 \quad (\text{B.5})$$

with data mean \bar{y}

χ^2 – chi-square

χ_{red}^2 – reduced chi-square, divided by number of degrees of freedom ν

R^2 – coefficient of determination

$0 \leq R^2 \leq 1$, “values can be less than zero”!. if $R^2 = 1 \rightarrow$ ideal fit; if $R^2 = 0 \rightarrow$ bad fit

$$R^2 = 1 - \frac{SSR}{TSS} \quad (\text{B.6})$$

“In case of a single regressor, fitted by least squares, R^2 is the square of the Pearson product-moment correlation coefficient relating the regressor and the response variable.” cite from wikipedia

Kolmogorov-Smirnov K-S-Test

B.4 other

minimum variance analysis (MVA)

determining magnetic cloud configuration ([Bothmer & Schwenn 1998](#))

hodogramm?

least-squares fit approximates mean linear regression

robust statistics

Non-parametric inferential statistical methods are mathematical procedures for statistical hypothesis testing which make no assumptions about the probability distributions of the variables being assessed. The most frequently used tests include - median - percentiles (quartiles) - Spearman’s rank correlation coefficient

histogram

generalized mean http://en.wikipedia.org/wiki/Generalized_mean

normal distribution

C Glossary

C.1 Astronomical constants

Astronomical unit: $1 \text{ au} = 149\,597\,870\,700 \text{ m}$ ([U.S. Nautical Almanac Office 2015](#))

Solar mass: $M_{\odot} = 1.9884(2) \times 10^{30} \text{ kg}$ ([U.S. Nautical Almanac Office 2015](#))

Nominal solar radius (photosphere): $R_{\odot} = 695\,700 \text{ km}$ ([Mamajek et al. 2015](#))

Sun escape velocity: $v_{\text{esc}} = 617.6 \text{ km/s}$ (Sun Fact Sheet...)

Solar rotation axis tilt: $i_{\odot} = 7.25^\circ$ ([U.S. Nautical Almanac Office 2015](#))

Solar surface rotation period at equator, sidereal: 25.05 d (Sun Fact Sheet...)

Nominal solar effective temperature (photosphere): $T_{\text{eff}\odot} = 5772 \text{ K}$ ([Mamajek et al. 2015](#))

C.2 Symbols

s/c - spacecraft

B - magnetic field strength

n - number density

...

C.3 Abbreviations

Projects:

AFFECTS Advanced Forecast For Ensuring Communications Through Space

HELCATS Heliographic Cataloging, Analysis and Techniques Service

FP7 Framework Programme 7

CGAUSS Coronagraphic German And US SolarProbePlus Survey

OPTIMAP OPerational Tool for Ionospheric Mapping And Prediction

Spacecraft:

SPP – Solar Probe Plus

WISPR – Wide-field Imager for Solar Probe

ACE – Advanced Composition Explorer

MAG – Magnetometer

SWEPAM – Solar Wind Electron Proton Alpha Monitor

RTSW – Real Time Solar Wind

SDO – Solar Dynamics Observatory

SOHO – Solar and Heliospheric Observatory

STEREO – Solar TErrestrial RElations Observatory

Organizations:

NASA – National Aeronautics and Space Administration

SPDF – Space Physics Data Facility

NOAA – National Oceanic and Atmospheric Administration

SWPC – Space Weather Prediction Center

UGOE – University of Göttingen

IAG – Institute for Astrophysics Göttingen

GFZ – GeoForschungsZentrum

WDC-SILSO – World Data Center-Sunspot Index and Long-term Solar Observations

Sun:

DB – disparition brusques (disappearing filaments?; quiescent filaments?)

C. Glossary

SSN – sunspot number

Solar wind:

IMF – interplanetary magnetic field

CME – coronal mass ejection

ICME – interplanetary coronal mass ejection

MC – magnetic cloud

HSS – high speed stream

CIR – corotating interaction region

SIR – stream interaction region

SB – sector boundary

BDE – bidirectional electrons

HCS – heliospheric current sheet

HPS – heliospheric plasma sheet

Earth:

Kp – planetare Kennziffer

Dst – Disturbance storm time

Coordinate systems:

GSE – geocentric solar ecliptic

GSM – geocentric solar magnetospheric

Theories and techniques:

MVA – minimum variance analysis

MHD – magnetohydrodynamic

GCS – Graduated Cylindrical Shell

CAT – CME Analysis Tool

References

- Bahcall, J. N., Pinsonneault, M. H. & Wasserburg, G. J. 1995, *Solar models with helium and heavy-element diffusion*, Reviews of Modern Physics, 67, 781, <http://adsabs.harvard.edu/abs/1995RvMP...67..781B>.
- Balogh, A. & Jokipii, J. R. 2009, *The Heliospheric Magnetic Field and Its Extension to the Inner Heliosheath*, Space Sci. Rev., 143, 85, <http://adsabs.harvard.edu/abs/2009SSRv..143..85B>.
- Banaszkiewicz, M., Axford, W. I. & McKenzie, J. F. 1998, *An analytic solar magnetic field model*, Astron. Astrophys., 337, 940, <http://adsabs.harvard.edu/abs/1998A%26A..337..940B>.
- Bartels, J. 1934, *Twenty-seven day recurrences in terrestrial-magnetic and solar activity, 1923-1933*, Terrestrial Magnetism and Atmospheric Electricity (Journal of Geophysical Research), 39, 201, <http://adsabs.harvard.edu/abs/1934TeMAE..39..201B>.
- . 1962, *Zur Vorgeschichte der Weltraumforschung*, Naturwissenschaften, 49, 313, <http://adsabs.harvard.edu/abs/1962NW.....49..313B>.
- Bartels, J., Heck, N. H. & Johnston, H. F. 1939, *The three-hour-range index measuring geomagnetic activity*, Terrestrial Magnetism and Atmospheric Electricity (Journal of Geophysical Research), 44, 411, <http://adsabs.harvard.edu/abs/1939TeMAE..44..411B>.
- Bartels, J. & Veldkamp, J. 1949, *International Data on Magnetic Disturbances, First Quarter, 1949*, J. Geophys. Res., 54, 295, <http://adsabs.harvard.edu/abs/1949JGR....54..295B>.
- Belcher, J. W., Lazarus, A. J., McNutt, Jr., R. L. & Gordon, Jr., G. S. 1993, *Large-scale density structures in the outer heliosphere*, Advances in Space Research, 13, 41, <http://adsabs.harvard.edu/abs/1993AdSpR..13..41B>.
- Billings, D. E. 1959, *Distribution of Matter with Temperature in the Emission Corona.*, Astrophys. J., 130, 961, <http://adsabs.harvard.edu/abs/1959ApJ...130..961B>.
- Bothmer, V. & Daglis, I. A. 2007, *Space Weather – Physics and Effects* (Praxis Publishing), <http://adsabs.harvard.edu/abs/2007swpe.book.....B>, doi:10.1007/978-3-540-34578-7.
- Bothmer, V. & Schwenn, R. 1998, *The structure and origin of magnetic clouds in the solar wind*, Annales Geophysicae, 16, 1, <http://adsabs.harvard.edu/abs/1998AnGeo..16..1B>.
- Bronstein, I. N., Semendjajew, K. A., Musiol, G. & Mühlig, H. 2000, *Taschenbuch der Mathematik* (Verlag Harri Deutsch), <https://books.google.de/books?id=zCKyuQAACAAJ>.
- Christensen-Dalsgaard, J., Gough, D. O. & Thompson, M. J. 1991, *The depth of the solar convection zone*, Astrophys. J., 378, 413, <http://adsabs.harvard.edu/abs/1991ApJ...378..413C>.
- Christensen-Dalsgaard, J., Dappen, W., Ajukov, S. V. et al. 1996, *The Current State of Solar Modeling*, Science, 272, 1286, <http://adsabs.harvard.edu/abs/1996Sci...272.1286C>.
- Cranmer, S. R. & van Ballegooijen, A. A. 2005, *On the Generation, Propagation, and Reflection of Alfvén Waves from the Solar Photosphere to the Distant Heliosphere*, Astrophys. J., Suppl. Ser., 156, 265, <http://adsabs.harvard.edu/abs/2005ApJS..156..265C>.
- Danziger, I. J. 1970, *The Cosmic Abundance of Helium*, Ann. Rev. Astron. Astrophys., 8, 161, <http://adsabs.harvard.edu/abs/1970ARA%26A...8..161D>.
- Elliott, H. A., Jahn, J.-M. & McComas, D. J. 2013, *The K_p index and solar wind speed relationship: Insights for improving space weather forecasts*, Space Weather, 11, 339, <http://adsabs.harvard.edu/abs/2013SpWea..11..339E>.

References

- Gurnett, D. A., Kurth, W. S., Burlaga, L. F. & Ness, N. F. 2013, *In Situ Observations of Interstellar Plasma with Voyager 1*, Science, 341, 1489, <http://adsabs.harvard.edu/abs/2013Sci...341.1489G>.
- Hapgood, M. A. 1992, *Space physics coordinate transformations - A user guide*, Planet. Space Sci., 40, 711, <http://adsabs.harvard.edu/abs/1992P%26SS...40..711H>.
- Hathaway, D. H. 2015, *The Solar Cycle*, Living Reviews in Solar Physics, 12, 4, <http://adsabs.harvard.edu/abs/2015LRSP...12....4H>.
- King, J. H. & Papitashvili, N. E. 2005, *Solar wind spatial scales in and comparisons of hourly Wind and ACE plasma and magnetic field data*, Journal of Geophysical Research (Space Physics), 110, 2104, <http://adsabs.harvard.edu/abs/2005JGRA..110.2104K>.
- Kivelson, M. G. & Russell, C. T. 1995, *Introduction to Space Physics* (Cambridge University Press), <http://adsabs.harvard.edu/abs/1995isp..book.....K>.
- Leitner, M., Farrugia, C. J., Möstl, C. et al. 2007, *Consequences of the force-free model of magnetic clouds for their heliospheric evolution*, Journal of Geophysical Research (Space Physics), 112, 6113, <http://adsabs.harvard.edu/abs/2007JGRA..112.6113L>.
- Lem, S. & Kandel, M. 1984, *His Master's Voice* (Houghton Mifflin Harcourt), <http://books.google.de/books?id=nzgLf4zKph0C>.
- Mamajek, E. E., Prsa, A., Torres, G. et al. 2015, *IAU 2015 Resolution B3 on Recommended Nominal Conversion Constants for Selected Solar and Planetary Properties*, ArXiv e-prints, arXiv:1510.07674, <http://adsabs.harvard.edu/abs/2015arXiv151007674M>.
- Maunder, E. W. 1904, *Note on the distribution of sun-spots in heliographic latitude, 1874-1902*, Mon. Not. R. Astron. Soc., 64, 747, <http://adsabs.harvard.edu/abs/1904MNRAS..64..747M>.
- McComas, D. J., Ebert, R. W., Elliott, H. A. et al. 2008, *Weaker solar wind from the polar coronal holes and the whole Sun*, Geophys. Res. Lett., 35, L18103, <http://adsabs.harvard.edu/abs/2008GeoRL..3518103M>.
- Miesch, M. S. 2005, *Large-Scale Dynamics of the Convection Zone and Tachocline*, Living Reviews in Solar Physics, 2, 1, <http://adsabs.harvard.edu/abs/2005LRSP....2....1M>.
- Newell, P. T., Sotirelis, T., Liou, K., Meng, C.-I. & Rich, F. J. 2007, *A nearly universal solar wind-magnetosphere coupling function inferred from 10 magnetospheric state variables*, Journal of Geophysical Research (Space Physics), 112, A01206, <http://adsabs.harvard.edu/abs/2007JGRA..112.1206N>.
- Newell, P. T., Sotirelis, T., Liou, K. & Rich, F. J. 2008, *Pairs of solar wind-magnetosphere coupling functions: Combining a merging term with a viscous term works best*, Journal of Geophysical Research (Space Physics), 113, A04218, <http://adsabs.harvard.edu/abs/2008JGRA..113.4218N>.
- Opher, M., Drake, J. F., Swisdak, M. et al. 2011, *Is the Magnetic Field in the Heliosheath Laminar or a Turbulent Sea of Bubbles?*, Astrophys. J., 734, 71, <http://adsabs.harvard.edu/abs/2011ApJ...734...71O>.
- Ossendrijver, M. 2003, *The solar dynamo*, Astron. Astrophys. Rev., 11, 287, <http://adsabs.harvard.edu/abs/2003A%26ARv..11..287O>.
- Owens, M. J. & Forsyth, R. J. 2013, *The Heliospheric Magnetic Field*, Living Reviews in Solar Physics, 10, 5, <http://adsabs.harvard.edu/abs/2013LRSP...10....5O>.
- Parker, E. N. 1958, *Dynamics of the Interplanetary Gas and Magnetic Fields.*, Astrophys. J., 128, 664, <http://adsabs.harvard.edu/abs/1958ApJ...128..664P>.
- Pizzo, V. J. 1991, *The evolution of corotating stream fronts near the ecliptic plane in the inner solar system. II - Three-dimensional tilted-dipole fronts*, J. Geophys. Res., 96, 5405, <http://adsabs.harvard.edu/abs/1991JGR....96.5405P>.

- Planck Collaboration, Ade, P. A. R., Aghanim, N. et al. 2016, *Planck 2015 results. XIII. Cosmological parameters*, Astron. Astrophys., 594, A13, <http://adsabs.harvard.edu/abs/2016A&26A...594A.13P>.
- Richardson, I. G. & Cane, H. V. 2012, *Near-earth solar wind flows and related geomagnetic activity during more than four solar cycles (1963-2011)*, Journal of Space Weather and Space Climate, 2, A2, <http://adsabs.harvard.edu/abs/2012JSWSC...2A..02R>.
- Richardson, I. G., Cliver, E. W. & Cane, H. V. 2000, *Sources of geomagnetic activity over the solar cycle: Relative importance of coronal mass ejections, high-speed streams, and slow solar wind*, J. Geophys. Res., 105, 18203, <http://adsabs.harvard.edu/abs/2000JGR...10518203R>.
- Richardson, J. D., Paularena, K. I., Lazarus, A. J. & Belcher, J. W. 1995, *Radial evolution of the solar wind from IMP 8 to Voyager 2*, Geophys. Res. Lett., 22, 325, <http://adsabs.harvard.edu/abs/1995GeoRL..22..325R>.
- Richardson, J. D. & Smith, C. W. 2003, *The radial temperature profile of the solar wind*, Geophys. Res. Lett., 30, 1206, <http://adsabs.harvard.edu/abs/2003GeoRL..30.1206R>.
- Schatten, K. H., Wilcox, J. M. & Ness, N. F. 1969, *A model of interplanetary and coronal magnetic fields*, Solar Phys., 6, 442, <http://adsabs.harvard.edu/abs/1969SoPh....6..442S>.
- Schwenn, R. 1983, *The average solar wind in the inner heliosphere: Structures and slow variations*, in NASA Conference Publication, Vol. 228, NASA Conference Publication, <http://adsabs.harvard.edu/abs/1983NASCP.2280.489S>.
- Schwenn, R. 1990, *Large-Scale Structure of the Interplanetary Medium*, ed. R. Schwenn & E. Marsch, Physics of the Inner Heliosphere I, 99, <http://adsabs.harvard.edu/abs/1990pihl.book...99S>.
- Thompson, M. J., Christensen-Dalsgaard, J., Miesch, M. S. & Toomre, J. 2003, *The Internal Rotation of the Sun*, Ann. Rev. Astron. Astrophys., 41, 599, <http://adsabs.harvard.edu/abs/2003ARA%26A..41..599T>.
- U.S. Nautical Almanac Office. 2015, *Astronomical Almanac for the Year 2016 and Its Companion, the Astronomical Almanac Online* (United States Department of Defense), https://books.google.de/books?id=Mc_VuQN_gVsC.
- Zhao, J., Bogart, R. S., Kosovichev, A. G., Duvall, Jr., T. L. & Hartlep, T. 2013, *Detection of Equatorward Meridional Flow and Evidence of Double-cell Meridional Circulation inside the Sun*, Astrophys. J., Lett., 774, L29, <http://adsabs.harvard.edu/abs/2013ApJ...774L..29Z>.

Acknowledgments

I thank

my supervisor Volker Bothmer
the committee (Ansgar Reiners, second?)
the proofreaders

The author like to thank the proofreaders for very helpful comments and suggestions.
the 'Büro' for cozily accomodating me all the long hours

for creating and making scientific data available:

- SWS list (see Acknowledgements in Elliott2013; directly Ian Richardson)
- OMNI data (see paper)
- ACE data
- Helios data (see paper)
- Kp data
- SSN data

I acknowledge the financial support from the projects

AFFECTS: Solar wind correlation with magnetosphere

CGAUSS: Solar wind model and extrapolation

HELCATS: Minimum variance analyses of magnetic clouds

OPTIMAP: Solar wind ACE time series

This work was done within the scope of the CGAUSS project, funded by the German Aerospace Center (grant number...).

The authors thank the Helios and OMNI teams for creating and making availabe the solar wind in situ data. The Helios and the OMNI data sets were supplied by the Space Physics Data Facility at NASA's Goddard Space Flight Center.

We thank the 'referees' for /important comments and suggestions. /careful review of this paper.

facilities/persons which made available the Helios and OMNI data

"Ian Richardson and Hilary Cane for making their Interplanetary Coronal Mass Ejection list readily available"

"Joseph King and Natalia Papitashvili for creating the combined OMNI data set"

The OMNI data were downloaded from NASA's Space Physics Data Facility ...

"We thank the reviewers for the careful review of this paper"

The Authors extend their thanks to the referee for important comments and suggestions.

This work was supported by the DLR CGAUSS project

We would like to thank XX for reading drafts of this manuscript...

This work has been done in the frame of the CGAUSS project (url), funded by the DLR

We would like to thank the Helios team and NASA's SPDF for supplying the plasma and magnetic field data (url)

The results presented in this thesis rely on the K_p index, calculated and made available by the German Research Centre for Geosciences in Potsdam from data collected at magnetic observatories. We thank the involved national institutes, the INTERMAGNET network and ISGI (isgi.unistra.fr).

Curriculum vitae

Malte Venzmer, born 5 February 1984 in Bremerhaven, Lower Saxony, Germany, finished secondary school (Abitur) at the Gymnasium Ganderkesee in 2003. Subsequently he performed his civilian service working in a care home for disabled persons in Westerland, Sylt.

In 2004 he began to study physics at the University of Konstanz. During his studies, in summer 2008, he did an internship at the Ångström Laboratory, Uppsala University, Sweden, working in the field of materials physics. In 2010/2011 he wrote his diploma thesis in the *Radio- and X-ray astronomy* group of Dr. Jürgen Kerp at the Argelander-Institute for Astronomy, University of Bonn. There, following his diploma in physics, he continued working under a scholarship until end of 2011.

In 2012 he started as a PhD candidate in the *Solar, heliospheric and space weather research* group of Dr. Volker Bothmer at the Institute for Astrophysics, University of Göttingen. During his doctoral studies he worked as a research assistant for several national and international projects. Most of his main results are described in this very thesis.

notes

Fragen:

- references vol # fett drucken?
- references journal kursiv drucken?
- maybe style references different. like in space science reviews?
- page # oben lassen?
- A5 format?

nice phrases:

...this leads to the question wh... . The answer to this question is developed in the course of the next section.

write basics without third persons view “we”

define if using astronomical symbols...

...and use style consistently

Letzte Änderungen:

Genehmigungen für die Abb. besorgen!!

check for topic sentences!

Am Anfang der Arbeit den folgenden logischen Aufbau der Kapitel erläutern.

Am Anfang jedes Kapitels den folgenden logischen Aufbau der Abschnitte erläutern.

Beides auf Änderungen überprüfen.

print figures to check look of colors

adjust figure width to textwidth...

complete pdfinfo text...

Abkürzungen CME, usw. konsequent nutzen und beim ersten Auftauchen ausschreiben.

englische Kommasetzung beachten!

schauen, ob Komma oder Punkte durch Semikolon ersetzt werden können

Prüfen, ob Überschriften den Inhalt des Kapitels gut beschreiben/gut zum Kapitel passen.

check if AE spelling consistently, search and replace: analyse, etc.

check for thin spaces in numbers with 5 digits and more

Header und footer für notes, Seitenzahl, Thema und Kapitel einfügen
check gnuplot plot text sizes and finish figures

check for changed links and update access date

sinnlosen Satz irgendwo einfügen

76 %, ACME irgendwo einfügen (ACME is good...)

comic strip aus thesis extrahieren

put movie in header or footer

create hyperref version including bibtex links

adjust link colors and remove boxes... (hyperref package options)

remove google-books links!

maybe adjust References like in Hathaway2010

LaTeX commands:

block commenting: strg+d

strg+shift+d

$$\frac{T_D}{[K]} = 21,8 \cdot \left(\frac{\Delta v_{FWHM}^{LMC}}{[\text{km s}^{-1}]} \right)^2 \quad (\text{C.7})$$

$$\frac{T_D}{[K]} = 21,8 \cdot \left(\frac{\Delta v_{FWHM}^{LMC}}{[\text{km s}^{-1}]} \right)^2 \quad (\text{C.8})$$

$$k = 3.56 \text{ e-6} \quad (\text{C.9})$$

$$k = 3.56 \cdot 10^{-6} \quad (\text{C.10})$$

$$k = 3.56 \times 10^{-6} \quad (\text{C.11})$$

1. CM LMC Longitude

drei CM LMC Latitude

Volume in $(^{\circ})^2 \text{m s}^{-1}$. Summe aller Voxel des Objektes.

Volume in $(^{\circ})^2 \text{m s}^{-1}$. Summe aller Voxel des Objektes.

- Volume

sdgffs CM GSR Velocity

label

asdf Volume

drei CM LMC Latitude

¹ oder ²

$$a^2 + b^2 = c^2 \quad (\text{C.12})$$

Formel zitieren: (Siehe Formel C.12, Formel (C.12), Seite 66)

package siunitx:
 $20.5 \times 10^{-3} \text{ kg}$
 $20.5 \times 10^{-3} \text{ kg}$
 $20.5 \times 10^{-3} \text{ kg}$

width defines the width of the resulting box as seen from the outside (This means it can be smaller than the material inside the box. You ~~can~~^{can} even set the width to 0pt so that the text inside the box will be typeset without influencing the surrounding boxes). Besides the length expressions, you can also use semi-log plots:

log-lin: logarithmic scale on the y-axis, and a linear scale on the x-axis

lin-log: logarithmic scale on the x-axis, and a linear scale on the y-axis

the naming is output-input (y-x), the opposite order from (x, y)

¹All listed websites were existent on 2008-09-15.

²All listed websites were existent on 2008-09-15.